International Journal of Progressive Sciences and Technologies (IJPSAT)
ISSN: 2509-0119.

https://ijpsat.org/

Vol. 50 No. 1 April 2025, pp. 01-26

Functional Qualification Comparison Studies Between The Preferentially Selected OPC And PPC Cements Produced In Nepal

Professor Dr. Anant Babu Marahatta[1,*], Puspa Kamal Dahal[2]

[1] Professor of Chemistry/[2]Student, Research and Innovation Unit, Kathford International College of Engineering and Management, Institute of Engineering, Tribhuvan University, Kathmandu, Nepal
*Corresponding author: abmarahatta@gmail.com

Abstract: One of the most eminent building composites used ubiquitously in diverse engineering arenas is concrete; a reinforced admixture comprising with the definite amount cements, aggregates, water, minerals, and many other supplementary cementitious materials. Among these ingredients, the quite indispensable one that vows to dispense exceptional hardening strengths and conformational stabilities with notable weather resiliencies is cement. Owing to its versatile clinker phases, severe kiln processes, and unequal temporal hydration/rehydration affinities leading to the production of discretely functioning chemical derivatives, the entire commercial markets across the globe consume its brands primarily as OPC and PPC. The exclusive reasons behind their variable hydration, plasticity, gluing, agglomerating, setting, hardening, and enduring potencies that are disclosed comprehensively via the spectroscopic microstructural assessment procedures still become a great dearth of evidences. This contribution utmost aims to address all these functional inequalities and dissimilar workability aptitudes of the OPC & PPC cement grains by accessing to their generic crystallite phases and microstructural coherent domains through XRD and FTIR spectroscopic means. The careful probing of the X-ray diffraction angles, scattering bands, basal spacing (*d*-space), band intensity & interferences superposition regimes, symmetry & spatial distribution range, net integral area & FWHM, crystallites sizes (L_c) & growth propensities, and number density of the closely stacked layers & edge plane thickness exemplify their disproportionate founding phases featuring the different packing ratio & interatomic layers crosslinking force, crystal defects & disorderliness, compressive & tensile strains, conglomeration cum grain size evolutions rates, adsorbing sites & exposable surface areas, etc. And, the rigorous judgements of the IR vibration bands and fingerprint regions deduce all those characteristic phases and their chemical moieties explicitly. These spectral interpretations not only declare their unalike functionalizing qualifications and cementitious features but also assure unidentical dissolution rates, hydration propensities, plasticity properties, and all the aftermath stiffening chemistries. We believe this insightful comparative analyses would be the leading industrial guidelines & consumer doctrines mainly for upgrading the specific cement brands & accreditations commercially.

Keywords: Spectroscopy, Crystallite phases, Crystal defects, Grain sizes, Adsorption site/area

1. INTRODUCTION

Cement is widely considered as the most ideal engineering material not only due to its versatile physicochemical characteristics but also comprising with the easy functionalizing crystallite phases exhibiting progressive hydration reactions generously vowing to produce a long term hardening products dispensing good environmental resiliency & structural durability, extra mechanical sustainability, exceptional compactness & compressibility, profound reinforcing & enduring ability, indispensable binding & conglomeration potentiality, etc. [1–3]. Based on the types of the multifaceted clinker phases undergoing with the severe kiln

processes, the chemical moieties derived from them, the variable consecutive hydration reactions affinities, and therewith produced disparate hydration product derivatives featuring the unequal plasticity, gluing, agglomeration, placing, adhering, setting, hardening, and concreting potencies, the cement materials are classified mostly as ordinary Portland cement (hereafter, OPC), Portland Pozzolana cement (hereafter, PPC), Portland slag cement, high alumina content cement, fast setting and quick hardening cement, etc. Among them, the OPC and PPC are two of the massively consumed cement materials globally (production: 4 bMt/yr (billion metric ton per year)) owing to their inconstant applications suitable for the multidisciplinary engineering arenas, viz. binding, plastering, joints-hardening, slabbing, masonry structures, pointing, shaping, concrete pavement, etc., and many other state-of-the-art molding crafts and hand carving art designs [3–5]. In the developing country like Nepal where the various ongoing mega construction projects across the nation intensify the national demands of the good quality cements pronouncedly, the rapid momenta gained more especially by the OPC & PPC cements and their high-tech production factories in appealing to the domestic and foreign investments are notably laudable (net investments: foreign ≈ $0.50 billion, and domestic ≈ $1.0 billion US) [6]; speculating that Nepal is equipped with the globally recognized cement production technologies, and has bound the manufacturers strictly within its ISO standard "Nepal Standard" (hereafter, NS) codes & guidelines [7, 8]. The flexible government policies and subsidiary schemes applicable to the both type investors, and prompt government supports for regularizing the clinker supplies, preserving the local raw materials and mine areas, establishing the national integrated clinker storage/production plants, and facilitating the import-export delicacy plans further surge the national and international interests in the Nepalese cement production factories [9,10]. The efficacies and effectiveness of these national efforts and governmental promotions are quite apparently visible in the entire Nepalese commercial markets as the both state owned and foreign aided industry produced OPC and PPC cement products are at most of publicly desirable types, and commercially preferable yet internationally incredible quality [8–10]. Saying this, the nationwide demand-supply trends of the state-made and Nepal imported OPC/PPC cements still remain undervalue: total capacity of cement productions = 15 mMt/yr (million), net integrative manufactures = 7.49 mMt/yr, bulk national demands = 9.05 mMt /yr, net imported in the year 2024= 500 kMt (thousand), and the commercial constructions across the nation are continually seeking for the NS codes and ISO norms satisfied brands of them. [7, 8, 11,12]. And, the in-depth R & D studies of them and therewith associated futuristic strategic plans required for upgrading the qualities of their cementitious features are still lacking. Present work intends to address the same to some extents with the basic aims of addressing disparate functional aptitudes of the OPC & PPC cements by assessing their microstructural coherent domains.

One of the most prevalent reasons of ongoing variable global demand rates of the OPC (annual growth rate = 29.18 % (projection years: 2024–2031))) [13(a)] and PPC (annual growth rate = 4.7% (projection years: 2022–2031)) [13(b)], and their export-import trends is because of their dissimilar functionalizing inclines and engineering functions. In particular, the (a) OPC has a higher heat of hydration and relatively faster setting time in the early stages; (b) PPC gains more compressive strengths over time while the OPC pledges for early strengths with good compressibility; (c) PPC withstands comparatively harsher weather conditions while the OPC exhibits less resiliencies in certain aggressive scenarios; (d) PPC has a less heat accumulation effects (thermal cracks) than the OPC; (e) OPC is usually preferable for the fast track constructions, and hence more abundantly found in the market while the PPC is mostly for long-lasting structures; (f) PPC is more cost-efficient, and eco-friendly than the OPC; (g) PPC has more finer grains than the OPC; and (h) PPC discards relatively more plasticizer, silica, alumina, etc. type additives. In fact, these discrete working functions of them are mostly determined by their precursor ingredients, industrial formulations & intermixing ratios, clinker phases & compositions, and the chemical additives added into them during the kiln processes: the OPC is basically prepared from the clinker phases (95%) and gypsum materials (5%) while the PPC is produced from the Pozzolanic materials (clinker (65%), gypsum (5%), and pozzolana (30%)) [1, 10, 14]. Unlike OPC, the PPC cement is manufactured with the more rigorous blending mechanisms: the blending materials are clinker particles, natural and non-natural pozzolana (5–25% by weight, sources: burnt-clay/shale/maize /rice husks/diatom shells & smectite clay (moler), calcined clay, direct deposits erupted from the active volcanos), and binary chemical compounds (slag and gypsum); or sometime it is produced directly by blending the OPC grains with the fly ash (CaO) and slag [10,14,15]. These generic disparities in the founding chemical phases make the PPC cement virtually better over the OPC in many engineering aspects: (a) mortar & concretes perdurabilities; (b) water permeability resistances & $Ca(OH)_2$ leaching blockages; (c) shrinkage controls & thermal expansions/ contractions; (d) hair-cracking & deep crevices preventions plus sudden cracklings lowering; (e) corrosion resistance to the reinforced iron bars and annealed iron wires etc. [15, 16]. These superior

International Journal of Progressive Sciences and Technologies (IJPSAT)
ISSN: 2509-0119.

https://ijpsat.org/
Vol. 50 No. 1 April 2025, pp. 01-26

functional properties acquired by the PPC made composites are because of the two interdependent successive hydration reactions pathways: the OPC ends its hydration reactions with the successful release of the primary C–S–H (I) silicate hydrate nanogel only whereas the PPC continues till the secondary C–S–H (II) silicate product is produced [17–19]. If their major chemical constituents (2CaO.SiO2 (belite, C2S), 3CaO.SiO2 (alite, C3S), and aluminates 3CaO.Al2O3 (C3A) derived from the specific clinker phases and auxiliary chemical formulations are referred, the former gel products of both of them are as a result of $C_2S + C_3S + C_3A +$ Water → C–S–H (I) + $Ca(OH)_2$ reaction, but the latter produced consecutively in the PPC-hydration only is typically due to $Ca(OH)_2$ + Fly Ash/Slag → C–S–H (II). The same secondary silicate gel of the PPC enables its concrete structures to gain extra endurances more progressively yet lately, and hence makes them more durable & long lasting relative to the OPC. Nonetheless, the either forms of the silicate hydrate gels can glue the mortar materials tightly and bind them adherently over the progressive increments of the hydration reaction time dispensing promising mechanical & thermal endurances plus chemical & weather resiliencies, but definitely in dissimilar extents in the discrete time periods & hydration stages.

The more eventual consequences associated with the unequal hydration chemical reactions affinities of the OPC & PPC at ambient temperature, and the nonequivalent cementitious aptitudes of their hydrated mortar pastes lie into the natures of the clinkers, clinker phases & auxiliary raw materials, generic crystallite phases and their quantities & qualities, particulates size distributions, hierarchical porosity & pore networks, adsorbing surface areas, crystallite sizes & growths propensities, water permeability & retaining capacities, etc. The only way to assess all these microstructural descriptors & their divergences in the OPC and PPC cements, and therewith consociated disparate workability and efficacy is to identify their predominant chemical moieties & functional motifs, clinker phases, and many other crystallites profiles. The various spectroscopic tools have showcased their abilities to quantify each of these microstructural attributes precisely both in the ultra-dry ready-to-use grainy states [20, 21] and hydrated mortar pastes forms [22, 23]. Present authors believe that the X-ray powder diffraction (hereafter, XRD) and Fourier transform infrared (hereafter, FTIR) spectroscopic profile assessments of the both Nepal made OPC and PPC crystallite phases, chemical moieties, and grainy dimensions & morphologies quantitatively in their ultrafine powder forms may provide the righteous pathways towards understanding their incomparable functions, contrasting serviceability, unequal functionalizing trends, and unsteady commercial fames. The ultimate findings may also serve as the effective guidelines indispensable for upholding the public trusts of them in the Nepalese commercial markets and their sustainable growths & developments plus appropriateness of the PPC brands over the OPC and vice versa for the particular engineering domain. To our knowledge, no comparative research works concentrated fully into the instrumental quantifications of the generic microstructural domains, granular disparities & discrepancies, and their diverseness present in the ultra-dry ready-to-use grainy matrices of the Nepal made OPC and PPC cements are reported. Taking into the considerations of these, this insightful work is worthy enough. The article is hereafter structured as: Material & Method in section 2, Result & Discussion in section 3, and Summary & Conclusion in section 4.

2. MATERIAL AND METHOD

2.1 Collection of the Cement Samples

We collected the required quantities of the four publicly desirable variable technology manufactured dry ready-to-use cement in powdered forms directly from the Kathmandu-based cement depots owned by the concerned manufacturers. Usually, the cement manufacturers construct their depots in the elevated areas wherein the high-density polyethylene made 50 kg cement sacs (Figure 1) are stored by stacking them one over the other partitioning with the waterproof polymeric sheets under the controlled humidity, dampness, and temperature conditions. Actually, they are known for the cement-storehouses designated more particularly for dispatching the general purpose OPC and PPC cements directly to the construction-sites as per the consumer needs and orders. For maintaining the confidentialities of the cement production plants & technologies, and declaring no conflict of interests among their products branded across the Nepalese commercial markets, the OPC and PPC cement specimens were named indiscriminately as OPC1 & PPC1 (manufacturer 1), OPC2 & PPC2 (manufacturer 2). The equal attentions were also given to their priory established industrial R & D characteristic features plus their catalogues based functioning properties & applicative aptitudes, and functionalizing qualifications & engineering appropriateness. Each grainy sample specimen was collected separately into the polyethylene bottles, and the aluminum foil layered stoppers were used securely to prevent it from the direct exposures to the humid

International Journal of Progressive Sciences and Technologies (IJPSAT)
ISSN: 2509-0119.

https://ijpsat.org/
Vol. 50 No. 1 April 2025, pp. 01-26

weather (Figure 1). Additionally, the physicochemical properties of the sample specimens were also preserved precisely, and ensured their grainy textures fully unaffected from the thermal & mechanical effects, mold & dampness, etc. In the time of declaring the particular cement brands of the OPC and PPC, the general surveys in regard to the (a) clinker & raw material qualities and their precursors, (b) popularity & market dynamics, (c) pre- & post- treatment attentions to their mortar pastes, (d) public consumptions rates & preferences, (e) environmental impacts & ecofriendly manufacturing technology, etc. were carried out.

2.2 Measurements of the X–ray Diffractograms

For the X-ray powder diffraction measurements, the fully sealed cement samples OPC1 & PPC1, and OPC2 & PPC2 of two different Nepalese manufacturers were submitted to Nepal Academy of Science and Technology (NAST); a government owned research organization offering the state-of-art instrumental facility to the academia and industrial sectors. At the time of sample registrations,

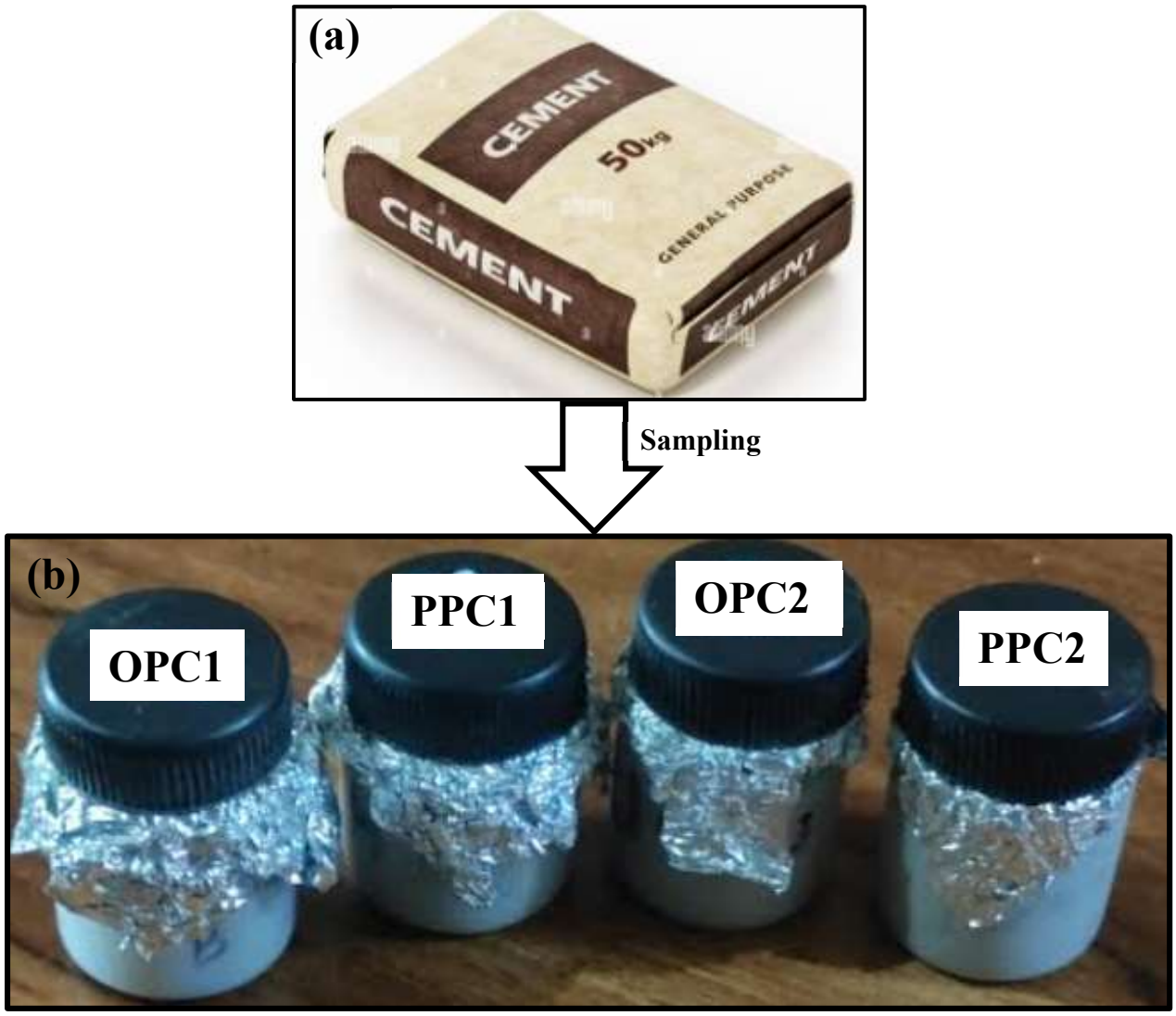

Figure 1. (a) The 50kg sac of general purpose cement available in the Nepalese commercial market, (b) an aluminum foil layered air-tight polyethylene bottles containing grainy powders of OPC1, PPC1, OPC2, and PPC2 cement sample specimens.

International Journal of Progressive Sciences and Technologies (IJPSAT)
ISSN: 2509-0119.

https://ijpsat.org/
Vol. 50 No. 1 April 2025, pp. 01-26

the designated technical operators were advised not to unseal the samples unless the XRD diffractometer is made functional. The diffractometer used for the present spectroscopic measurements was BRUKER D2 PHASER; a bench-top instrument equipped with the unique detector and digital monochromator mode for any unwanted sample florescence & background scatterings, and can deliver relatively high quality data with rapid assembling rates. In measuring the XRD spectral patterns within the angular range 2θ = 10–90°, a step size of an angular increment $\Delta\theta$ = 0.02°, and a material scanning rate of 0.5°/min were set as per the operational guidelines of the diffractometer. And, the number of counts (intensity) vs X-ray diffraction angles ($2\theta^{o}$) (coupled two theta/theta) of the entire crystallite phases were recorded as X-ray diffractogram for each sample specimen separately. Based on the objectives set for the present studies, all the diffractograms were plotted so as to compare the diffraction patterns and therewith associated crystallite-phases in relative scales.

2.3 Measurements of the FTIR Spectrograms

Alike to the XRD measurements, the four cement samples OPC1, OPC2, PPC1, and PPC2 delivered to the NAST were also used for the FTIR spectral measurements. The concerned instrumental operators were asked to unseal each of the samples turn by turn just before mixing the cement grains with the KBr powder (a sample carrier offering an optically transparent feature within the IR frequency range of the FTIR spectrophotometer) in the ratio 99:1 (by weight). The special molding and hydraulic pressure set was employed while pressing the mixture into the disc, and the fine KBr–pellet of every sample specimen was prepared for the spectral measurements. The FTIR spectrophotometer was of 'Shimadzu IR Tracer□100' model; a high precision instrument equipped with the outstanding measurement speed, sample sensitivity, and spectral resolutions with easy-to-use analytic tools. The spectrophotometer was finely calibrated at ambient air conditions, and its internal functions were made standardized as per the operational guidelines. In every spectral measurements, the KBr-pellet of the particular cement sample was fed into the spectrophotometer, and the concerned interferogram was recorded within the instrumental range of absorption frequency = 400 cm^{-1}–4000 cm^{-1}, resolution limit = 4 cm^{-1}, and the sample scanning rate = 50/sample. The Fourier transform technique was applied while converting the concerned interferograms into the easy-to-interpret IR spectrograms. Alike to the XRD diffractograms, all the IR spectrograms were plotted for the sake of comparing the fingerprint spectral bands of all the chemical fragments & functional moieties present in the particular crystallite phases of the OPC and PPC cements explicitly.

2.4 Determination of XRD-Profile Descriptors

In order to find out the XRD-profile descriptors such as spectral band positions at particular diffraction angles (θ^{o}), interatomic-layer distance (d), minimum crystallite- (L), grain-, and particle- sizes of the most predominant crystallite phases of all the four cement samples, we at first identified their most intense XRD peaks at the specific diffraction angles ($2\theta_{max}{}^{0}$), and retrieved the required datasets (intensity vs peripheral angles of the $2\theta_{max}{}^{0}$) explicitly. Each dataset for each sample specimen was assessed with the Microsoft Excel spreadsheet, and the corresponding spectral band was fitted with the standard *Gaussian* convolution curve separately. The Cartesian coordinates that generate the 3D spatial protrusion and normal distribution of the *GAUSS* function were produced programmatically, and the required parametric standardizations were carried out as per the needs of the peak-fitting procedures. The controlling parameters such as peak height (H), peak width (W), and full-width at half-maximum (herewith, FWHM (β^{0})) were directly linked to the normal distribution patterns of the *GAUSS* convolution, and the particular value for each of them was inserted explicitly till the optimum peak-fitting between the particular XRD band and the *Gaussian* curve was achieved. The extent of the normal distributions acquired by the thus fitted XRD band was also taken into account while estimating the FWHM regime. The net integral area (A) (mm^2) lying under all the best-fitted XRD bands was determined using the mathematical relation shown in Eq. 1.

$$A = \frac{H \times \beta}{0.3989 \times 2.35} \quad (1)$$

The diffraction angles assigned to the most prominent ($\theta^0 = 2\theta_{max}{}^0/2$) as well the subsidiary ($\theta^0 = 2\theta^0/2$) spectral bands of each cement sample were substituted in Bragg's equation (Eq. 2), and the interatomic-layer distance d (*d*-space, basal spacing) for every crystallite phases was determined.

$$n\lambda = 2d\,sin(\theta) \quad (2)$$

Where;

n = order of diffraction,

λ = wavelength of the incident X-ray (λ = 1.54 Å),

θ = angle of incidence

And, the β-value determined for the most intense XRD band only of all the samples was substituted in Eq. 3 for estimating the crystallite size L_c of their predominant crystallite phases.

$$L_c = (K \times \lambda)/(\beta \times cos(\theta)) \quad (3)$$

Where;

K = Scherrer's constant,

The numeral value for the K was obtained from the relation formulated in Eq. 4; a formula referred mostly for the cases where the (a) β is determined through the *Gaussian* peak fitting technique, and (b) material to be investigated contains maximum percentage spherical particulates (the cement grains mostly contain optimum proportions spherical particulates) [14, 24].

$K = 2\sqrt{(\ln 2)/\pi} \cong 0.9394$ [25, 26] (4) Thus calculated values of the L_c and d for every sample specimens were substituted in Eq. 5, and the corresponding number of the parallel interatomic planes m stacked one over the other representing edge plane thickness of the particular crystallite phases were approximated.

$$m = \frac{L_c}{d} \quad (5)$$

3. RESULT AND DISCUSSION

3.1. OPC vs PPC Cements: Spectroscopic Interpretations

3.1.1. Grainy Properties and Effectiveness of the XRD Method

The exclusive presence of the generic crystallite phases in the granular cores of the grainy OPC and PPC cement matrices always become the most versatile means of assessing their disparate workability, compressibility, enduring abilities, hydration affinities, particulates compactness, environmental and thermomechanical resiliencies, etc. [22, 23]. Besides these, the size of the founding crystallites and their development & growth propensities, agglomeration tendencies, coarse aggregations, granular textures & hierarchical porosities, and many other closely interdependent microscopic structures serve as the indispensable credentials deterministic to their multifaceted cementitious features and multidimensional engineering functions. More than this, the extents by which the heat of hydrations of the OPC/PPC cements occur, and the kinematics of their progressive rehydration chemical reactions upon the pre- and post- treatment with water to their mortar pastes plus therewith associated consecutive setting chemistries and engineering attributes are directly dependable assets on the average grain size distribution ranges, intergranular complexities, water wettability and permeability tendencies, water diffusions and particulates endosmosis phenomena, evaporable water (absorbed and capillary water) retaining and interlocking abilities of the pore networks, etc. [20–23]. In fact, all these microstructural attributes vow to measure the dissimilar functioning abilities and functionalizing qualifications of the OPC and PPC cements both in the ultra-

International Journal of Progressive Sciences and Technologies (IJPSAT)
ISSN: 2509-0119.

https://ijpsat.org/
Vol. 50 No. 1 April 2025, pp. 01-26

dry as well as in hydrated mortar pastes forms. Though the actual setting chemistries and the hardening aptitudes of them are also the direct functions of the water-cement (w/c) intermixing ratio, post-curing frequencies with water, temporal hydration kinetics, types of the C–S–H silicate hydrate nanogels and their plasticity, etc. [23], the thorough spectroscopic investigations and comparative quantitative assessments of their granular cores & particulates compactness, and the exact crystallite profiles always provide the in-depth insights inevitable to understand their disparate cementitious functions and engineering attributes. Owing to these pivotal roles of the microstructural domains in offering promising cementitious features, present authors employed the powder-XRD spectroscopy and the closely interlinked mathematical subordinates herewith, and assessed the exclusive crystallite profiles of the preferentially selected OPC1 & PPC1 cements of one manufacturer, and the OPC2 & PPC2 of another manufacturer in their ultra-dry ready-to-use grainy powder forms. Being this spectroscopy a quite esteemed nondestructive method more especially in characterizing the materials comprising with the particular crystallite phases like in the cements, therewith predicted functioning abilities and applicative qualifications of the OPC and PPC become the fair means of rating their unequal functionalizing inclines. The following subsections discuss the same in relative scales subsequently.

3.1.1.1 XRD Peak Positions

The diffraction angular positions ($2\theta^{o}$) designated to the most prominent XRD bands of the both type OPC and PPC cement samples are listed out in Table 1, and those that are assigned to their subsidiary spectral bands are presented comparatively in Table 2. Additionally, the complete diffractograms for them exhibiting the contrasting diffraction patterns at the particular angular positions are shown in Figure 2 and Figure 3 wherein the most intense peak position ($2\theta_{max}{}^{0}$) and the X-ray intensity recorded as "counts per second" are mentioned separately in their insets for the sample sets OPC1 & PPC1, and OPC2 & PPC2 respectively. According to their diffraction angles ($2\theta^{o}$) and therewith identified crystallite phases (abbreviated with the non-repetitive symbols just for the simplicity) compared in the Table 2, the quite contrasting founding chemical compositions and the clinker phases are clearly observed in OPC and PPC cement specimens. In the course of characterizing all these disparate spectral patterns and diffraction angular positions, we fully referred to the databases assembled in the complete guides to the crystallite phases and chemical compounds of interests in the cements and concrete research available elsewhere [23, 27, 28]. The absolute inclusions of these chemical phases and the functional constituents plus the exclusive comparisons between them make us to theorize that the microstructural functional domains and the premiere applicative qualifications of the Nepal made OPC and PPC cements are manifestly quite different, and so are their dissimilar functionalizing qualifications and functioning aptitudes at the distinctive functionalizing scenarios and aggressive engineering conditions. For example, the sample PPC1 has a few distinctive diffraction bands in between the 2θ angles 21.2º to 29.9º

Table 1. Comparisons of the $2\theta_{max}{}^{0}$ based d-space, predominant crystallite phases, L_c-value, and band-area between OPC1 & PPC1, and OPC2 & PPC2 cement samples. Abbreviations: C = Calcite, Ar = Arsenate, C_2S = α-Dicalcium Silicate, CS = β-Dicalcium Silicate, P = Portlandite, A = Alite, Ag = Aragonite, V = Vaterite, G = Gypsum.

Cement samples	XRD peak Positions (º)		*d*-space (*nm*)	Crystallite phases	FWHM (β) (°)	Band-area (A) (mm^2)	Crystallite size (L) (*nm*)	No. of parallel planes (m)
	$2\theta_{max}$	θ_{max}						
OPC1	33.65	16.83	0.223	C,Ar,C_2S,CS	0.2237	196.17	38.73	174
PPC1	27.15	13.57	0.181	P, A, Ag, V	0.2661	443.53	32.06	177
OPC2	32.38	16.19	0.215	C, G	0.2119	186.74	40.75	190
PPC2	26.92	13.46	0.179	P, A, Ag, V	0.2355	305.22	36.21	202

but the OPC1 has the foremost band at 2θ = 30.5º; specifying that alite ($3CaO.SiO_2$ or C_3S), fly ash (CaO), portlandite ($Ca(OH)_2$), aragonite, vaterite (one of the three polymorphs of $CaCO_3$ (calcite, aragonite, and vaterite)), and gypsum ($CaSO_4.H_2O$) phases are

International Journal of Progressive Sciences and Technologies (IJPSAT)
ISSN: 2509-0119.

https://ijpsat.org/
Vol. 50 No. 1 April 2025, pp. 01-26

majorly present in the PPC grains. Similarly, unlike in the OPC1, the disparate XRD peaks of the PPC1 at $2\theta = 34.7^{o}$ (portlandite, belite ($2CaO.SiO_2$ or C_2S), calcium aluminoferrite ($4CaO.Al_2O_3.Fe_2O_3$)), 41.8^{o} & 43.4^{o} (aragonite, gypsum, arsenate ($AsO4^{3-}$ unit bearing chemical moieties: $CaH_4(AsO_4)_2$, CaH (AsO_4), $Ca_3(AsO_4)_2$, and $Ca_5(AsO_4)_3OH$)), 52.3^{o} (alite, portlandite), 60.3^{o} & 62.8^{o} (hatrurite derived alite phases), 68.7^{o} (traces of silica (SiO_2, α-quartz)), etc. may confirm its nonidentical chemical features and crystallites compositions both in the non-hydrated grainy forms and hydrated mortar paste matrices. Alike to these differences, the basic structural units and their most probable functional attributes compared in between the OPC2 and PPC2 specimens are also quite prevalent but not so much distinctive to that of the OPC1 and PPC1 as the X-ray diffraction patterns for the OPC1 & OPC2, and PPC1 & PPC2 are procreating each other in an almost identical manner as depicted in Figure 4. In this contribution, we neither concentrate fully into the spectral patterns of the OPC-only and PPC-only cement samples nor analyze their brands quality and accreditations as the present objective is solely aimed to compare their functional qualifications and workability rather characterizing their isolated spectral patterns and diffraction angles individually. The interested researchers can access to our previous research articles published elsewhere [23, 29, 30] for the insightful understanding of the Nepal made dissimilar brands OPC /PPC cements and their most probable characteristic physicochemical features in their grainy morphological textures and hydrated mortar pastes forms.

3.1.1.2 XRD Derived *d*–space Value

The X–ray diffraction angles are highly useful to identify the lattice space of the corresponding crystallite phases (002 plane) that are known to give rise to the distinctive spectral bands with recognizable intensity at the specific diffraction angular regimes. The Bragg's equation formulated in the Eq. 2 is frequently used mathematical means of measuring their *d*-space value; a primary descriptor indispensable for describing the packing ratio, ratio of the basal planes, and void-volume of the specific type crystallite phases [20]. The same is usually taken as the most significant indicator applicable not only to reconfirm the individual crystallite phases present in the cement grains but also to envision their crystallographic arrangements vowing to provide the intergranular space occupancy and interatomic layers spacing [21]. In fact, the particle packing propensities and compressing densities plus the capillary water permeation and thereafter occurring overall chemical hydration and rehydration affinities of the cement grains are directly dependable cementitious features on the microstructural intermittent spacing exist in between the interatomic layers of the disproportional crystallite phases, the precise determinations of the *d*-space values in each of the phases directs us towards the righteous pathways of speculating net functional disparities and variable applicative qualifications of the dissimilar brand cements. The Bragg's formula calculated *d*-space values for each and every crystallite phases characterized in the Nepal made OPC1 & PPC1, and OPC2 & PPC2 cement samples in their grainy ultrafine powder matrices are summarized in the Table 2. Therein, the most probable distinctive crystallite phases identified on the basis of the priory established $2\theta^{o}$ literature values and standard *d*-space spectral databases [23, 27, 28], and the relative abundancies of them are compared exclusively. For simplicity, the $2\theta_{max}{}^{o}$ diffraction angular band based *d*-space values are sorted out separately in the Table 1 for pinpointing the most predominant crystallite phases present in the both OPC and PPC cements. The intensive comparisons among the particular *d*-space values assigned to the particular crystallite phases mark that the PPC and OPC type cements have few additional yet contrasting crystallite phases comprising with the uniquely spaced interatomic layers and unequally packed crystallographic structures. For example, the crystallite phases alite, belite, fly-ash, portlandite, vaterite, calcite, aragonite, etc. of the PPC cements have the *d*-space values less than 0.20 nm but none of the chemical phases present in the OPC cements have such a low regime intermittent spacing. And, the crystallite phases such as bassanite, aphthitolite, *α*–dicalcium silicate, tricalcium aluminate, calcium aluminoferrite, etc. present only in the OPC cements have the *d*-space value in the range 0.35 nm–0.40 nm, and the alite (hatrurite) & silica (α-quartz) phases present only in the PPC have that value in 0.39 nm–0.44 nm range. These crystallite profiles implicate us that there is the existence of the disparate functional roles of the OPC and PPC cements in the apparent engineering conditions. After the careful crosschecking of all these *d*-space values listed in the Table 2, we found none of them deviated quite far from the related literature datasets: belite & calcite, d = 0.21 nm–0.27 nm; alite & calcite, d = 0.16 nm–0.31 nm; gypsum, d = 0.23 nm; arsenate, d = 0.28 nm–0.30 nm; portlandite, d = 0.27 nm; aragonite & vaterite, d = 0.27 nm–0.29 nm; calcium arsenate, d = 0.29 nm and 0.22 nm; ettringite (calcium aluminium sulfate) d = 0.22 nm–0.39 nm; silica, d = 0.43 nm [20, 21, 27]. These resemblances ensure us that the present spectral profile assessments and the related mathematical calculations lie somewhat in the better precisions level.

International Journal of Progressive Sciences and Technologies (IJPSAT)
ISSN: 2509-0119.

https://ijpsat.org/
Vol. 50 No. 1 April 2025, pp. 01-26

Table 2. Comparisons of the $2\theta^{o}$ diffraction angles of the characteristic XRD-bands, *d*-space, and therewith associated crystallite phases between the OPC1 & PPC1, and OPC2 & PPC2 cement samples. Abbreviations: A = Alite, B = Belite, C = Calcite, G = Gypsum, Ag = Aragonite, V = Vaterite, P = Portlandite, As = Fly ash, Ar = Arsenate, Ah = Alite (Hatrurite), Si = Silica (α-quartz), Ph = Pharmacolite, M = Magnesium oxide, Ca = Calcium oxide, G = Gypsum, Ba = B*assanite,* Ap = Aphthitalite, C_2S = α-Dicalcium Silicate, CS = β-Dicalcium Silicate, C_3A = Tricalcium Aluminate, C_3S_2 = Tricalcium Disilicate, SH = γ-Dicalcium Silicate Hydrate, CA_2 = Calcium Dialuminate, Cf = Calcium Aluminoferrite.

OPC1		PPC1			OPC2		PPC2		
$2\theta^{o}$	*d*-space (*nm*)	$2\theta^{o}$	*d*-space (*nm*)		$2\theta^{o}$	*d*-space (*nm*)	$2\theta^{o}$	*d*-space (*nm*)	
30.5	0.203 (M)	21.2	0.142 (A, As)		29.5	0.196 (P, Cf)	21.2	0.142 (A, As)	
33.6	0.223 (C, Ar, C_2S, CS)	27.2	0.181 (P, A, Ag, V)		32.3	0.215 (C, G)	26.9	0.179 (P, A, Ag, V)	
35.4	0.234 (Ca)	29.9	0.198(G,A,C)		32.7	0.217 (C, Cf)	29.7	0.197 (G,A,C)	
37.8	0.249 (Si)	30.6	0.203		34.4	0.228 (C, Cf)	32.4	0.215	(C,
39.9	0.263 (C)	32.6	0.216	(M,	36.8	0.244 (Ag)	32.9	0.218	G)
42.3	0.278 (Ca, Cf, CS, C_3A)	33.1	0.219	C, G)	38.9	0.257 (C_3S_2)	34.7	0.229 (P, A, B, Cf)	
43.9	0.288 (Ph,Ar)	34.7	0.229(P, A, B, Cf)		41.5	0.273 (B)	39.7	0.262 (C)	
48.1	0.314 (G)	39.9	0.263 (C)		44.2	0.289(Ph,Ar)	41.6	0.273 (Cf)	(A,B
50.8	0.330 (V)	41.8	0.275	(A,	45.9	0.301 (A)	43.1	0.283 (Cf)	Ar, Ag,
52.8	0.343 (Ba)	43.4	0.285	Ag,G Ar,B, Cf)	47.2	0.308 (SH, P, CA_2)	46.1	0.301	G)
57.5	0.370 (Ap)	50.7	0.329	(A,P)	50.1	0.326 (Ag)	47.5	0.310	
60.9	0.391(C_2S,Cf)	52.3	0.339		51.9	0.337 (C_3A)	50.5	0.328	(A,
63.2	0.404 (C_3A)	57.5	0.370	(P)	56.7	0.366 (SH)	52.1	0.338	P,V)
—	—	60.3	0.387	(Ah,	60.2	0.386 (C_2S)	56.6	0.365 (P)	
—	—	62.8	0.401	C_3A)	62.6	0.401 (C_3A)	60.3	0.387	(B,Ah
—	—	68.7	0.435 (Si)		—	—	62.8	0.401	C_3A)
—	—	—	—		—	—	68.5	0.433 (Si)	

The crucial functional properties abstracted from all these dissimilar regimes nanometer range *d*-space interlocking crystallite phases are in general more relevant for comparing the working efficiencies of the OPC and PPC cements: the mechanical, thermochemical, heat resiliencies, hair-cracking prevention, extreme weather stabilities, durability & endurance, dimensional stability & mechanical strengths, etc. of the resulting concrete structures are directly dependable accredits on the founding crystallite phases of dissimilar proportions & chemical compositions, and their progressive hydration & rehydration reactions affinities. To these engineering attributes and functional domains, the tightly packed crystallite phases cum smaller *d*-space chemical phases alike to those found predominantly in the PPC grains contribute far better efficacies, effectiveness, and workability than the crystallite phases having the relatively larger *d*-space values. For examples, the major chemical phases of the PPC cements characterized with the smaller *d*-space values usually showcase the optimal level functions such as: (a) alite (C3S) is fully responsible for the early strength development of the concrete (faster hydration), (b) belite (C_2S) contributes a lot for acquiring the late strength, long-lasting,

and durability (late hydration) of the structures, (c) fly ash (CaO) improves the plasticity, placing, setting, and hardening abilities of the mortar pastes, (d) portlandite ($Ca(OH)_2$) offers better mechanical strengths and influences the pore structures of the hydrated mortars, (e) vaterite (μ–$CaCO_3$) enhances the binding abilities in the concrete hardened mixtures, (f) calcite ($CaCO_3$ (*hex.*)) acts as an inert–filler for the promising setting performances, (g) aragonite ($CaCO_3$ (*o.–rh.*)) nanocrystals magnify the cement strengths and mechanical resiliencies, etc. But, the minor proportions crystallite phases of them characterized with the larger *d*-space values are involved in pledging very minimal functional contributions such as: (a) bassanite ($2CaSO_4.H_2O$) simply influences the setting time and early strengths, (b) aphthitolite $(Na, K)_2SO_4$ provides compressibility and expansion stability strengths, (c) α–dicalcium silicate (Ca_2SiO_4; α-C_2S) resists the chemical and weather attacks, (d) tricalcium aluminate ($Ca_3Al_2O_6$; C_3A) contributes to the rapid hardening processing, (e) calcium aluminoferrite ($Ca_4FeA1_3O_{10}$) simply offers the satisfactory strengths along with lowering melting points of the raw materials in clinker production stages, etc. The same logical interpretations can be abstracted from the real-world crystallite phases of the unequal *d*-space values identified in the OPC type cement samples (Table 2), but the cementitious functions offered by the alite, belite, fly ash, portlandite like chemical phases are still noted highly prevalent in the PPC. The ultimate conclusion we can derive from these comprehensive spectral analyses is unequal quantities and reciprocal proportions plus variable chemical compositions of the wide range crystallite phases always determine the extents by which the OPC/PPC cements and their mortar pastes & concrete matrices acquire the cementitious features successively. The hydration reactions of them that lead to produce the nanogel glues such as $C_2S + C_3S + C_3A + Water \rightarrow C–S–H\ (I) + Ca(OH)_2$ (OPC and PPC), and $Ca(OH)_2$ + Fly Ash/Slag → C–S–H (II) (PPC only) also demonstrate the same dependencies of their unequal plasticity features and setting chemistries on the reacting crystallite phases, and hence verify that they appeal for unequal rate engineering functions and functionalizing traits. To some extents, the most predominant and the auxiliary crystallite phases held into them can be quantified by measuring the net area (A) lying under their own individual diffraction bands which are, however, practically infeasible. Therefore, we have simply approximated the quantities of their most predominant crystallite phases through the *GAUSS* function peak-fitting procedures, *Gaussian* like normal distributions mappings, and the peak-area estimations (subsection 3.1.1.3).

International Journal of Progressive Sciences and Technologies (IJPSAT)
ISSN: 2509-0119.

https://ijpsat.org/
Vol. 50 No. 1 April 2025, pp. 01-26

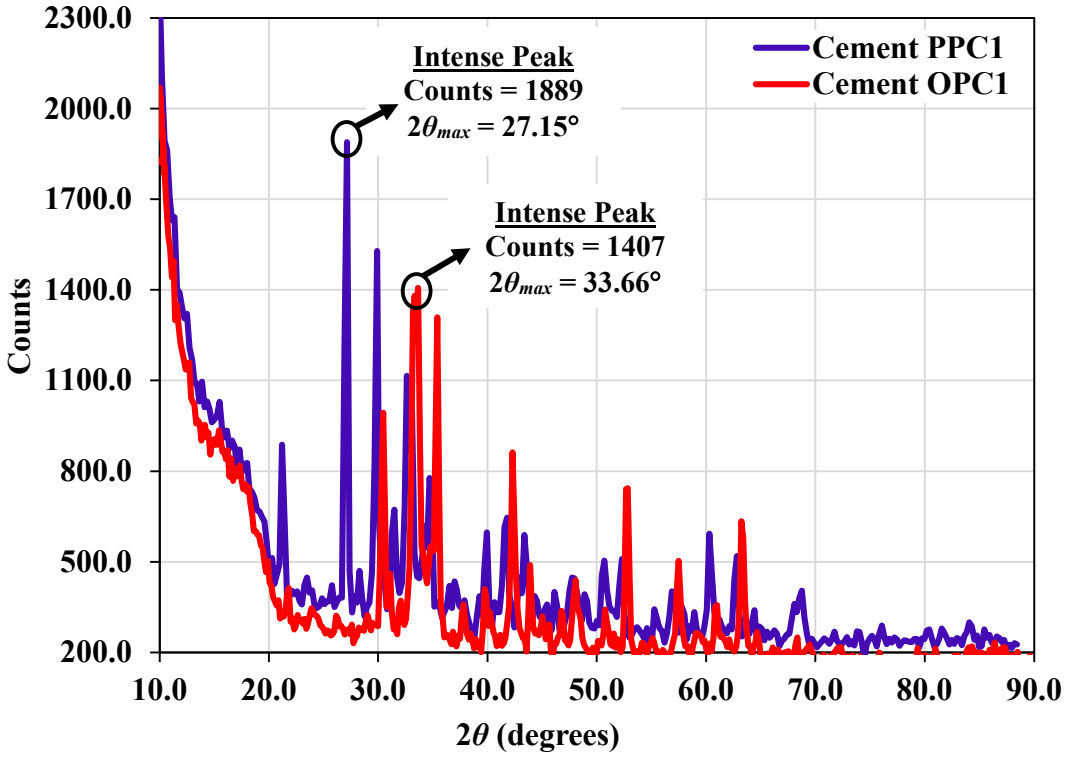

Figure 2. Comparison of the XRD diffractograms for the cement samples OPC1 and PPC1 produced by the same manufacturers. The most intense spectral bands assigned to the predominant crystallite phases are marked with their maximum count values and $2\theta_{max}$°. The *Gaussian* convolution fitting for each of them are shown in Figure 3.

International Journal of Progressive Sciences and Technologies (IJPSAT)
ISSN: 2509-0119.

https://ijpsat.org/
Vol. 50 No. 1 April 2025, pp. 01-26

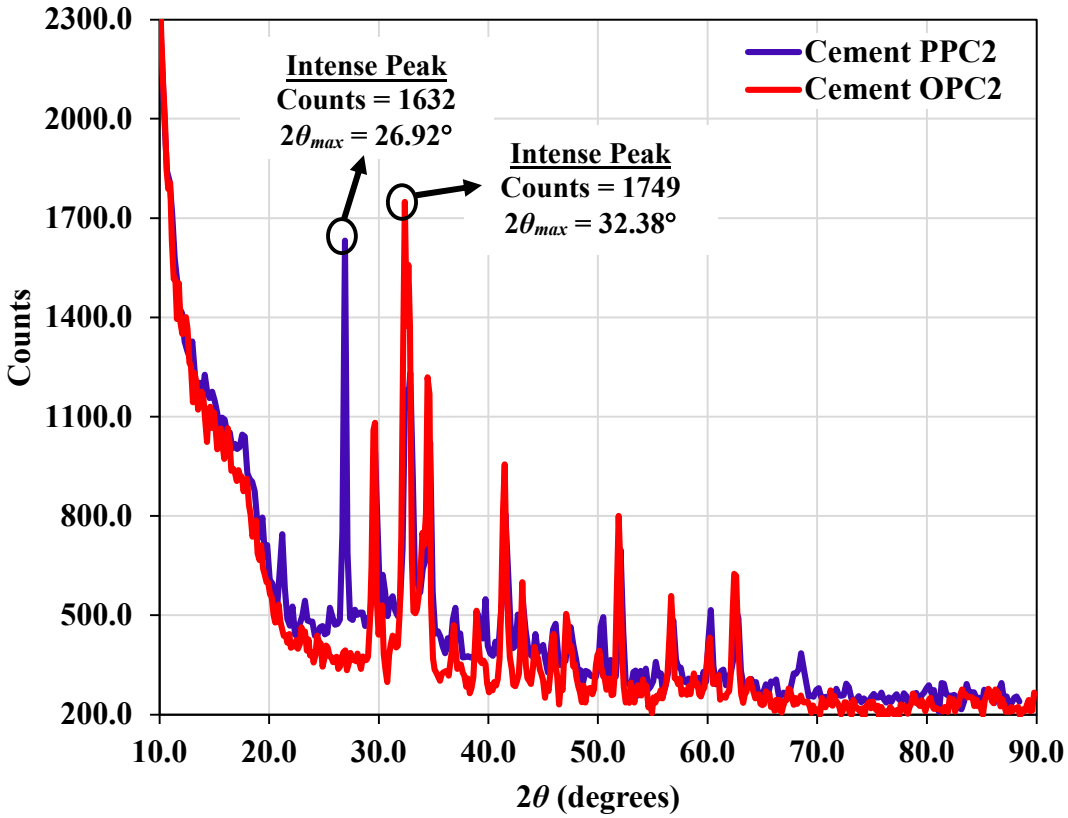

Figure 3. Comparison of the XRD diffractograms between the cement samples OPC2 and PPC2 produced by the same manufacturer. The most intense spectral bands assigned to the predominant crystallite phases are marked with their maximum count values and $2\theta_{max}$°. The *Gaussian* convolution fitting for each of them are shown in Figure 3.

3.1.1.3 Area (A) and Symmetry Analyses of the XRD Bands

In general, the exact estimation of the quantitative amounts of the crystallite phases present in the cement materials through the net integral area approximations of their corresponding XRD bands is practically inappropriate as the same crystallite phases may diffract the X–ray beam at multiple angular regimes ($2\theta^{o}$) based on their crystal structures and unit-cell alignments but definitely with contrasting total diffracted intensity, counts per second, spectral height & width, spectral acuteness /obtuseness, *Gaussian* like normal spatial distribution, etc. However, the underlying principle "the integral area under the any XRD band is directly proportional to the total diffracted intensity, and the degree of diffraction is a direct function of the crystallites scattering factors" allows us to quantify the crystallite phases by approximating the net area under their particular spectral bands arousing at the typical diffraction angle [31, 32]. Additionally, the intensity of the XRD peak is highly deterministic to the atomic scattering factors, atomic layouts & configurations, and the overall crystallographic geometrical arrangements of the unit-cells in the particular crystallites, the somewhat accurate approximations of the net integral area under the specific predominant XRD bands vow us to assess the

International Journal of Progressive Sciences and Technologies (IJPSAT)
ISSN: 2509-0119.

https://ijpsat.org/
Vol. 50 No. 1 April 2025, pp. 01-26

quantitative proportions of the concerned crystallite phases tentatively. The peak fittings between the *GAUSS* function convolution and the most prominent XRD bands of the particular crystallite phases of the OPC and PPC cements are shown in Figure 5, and

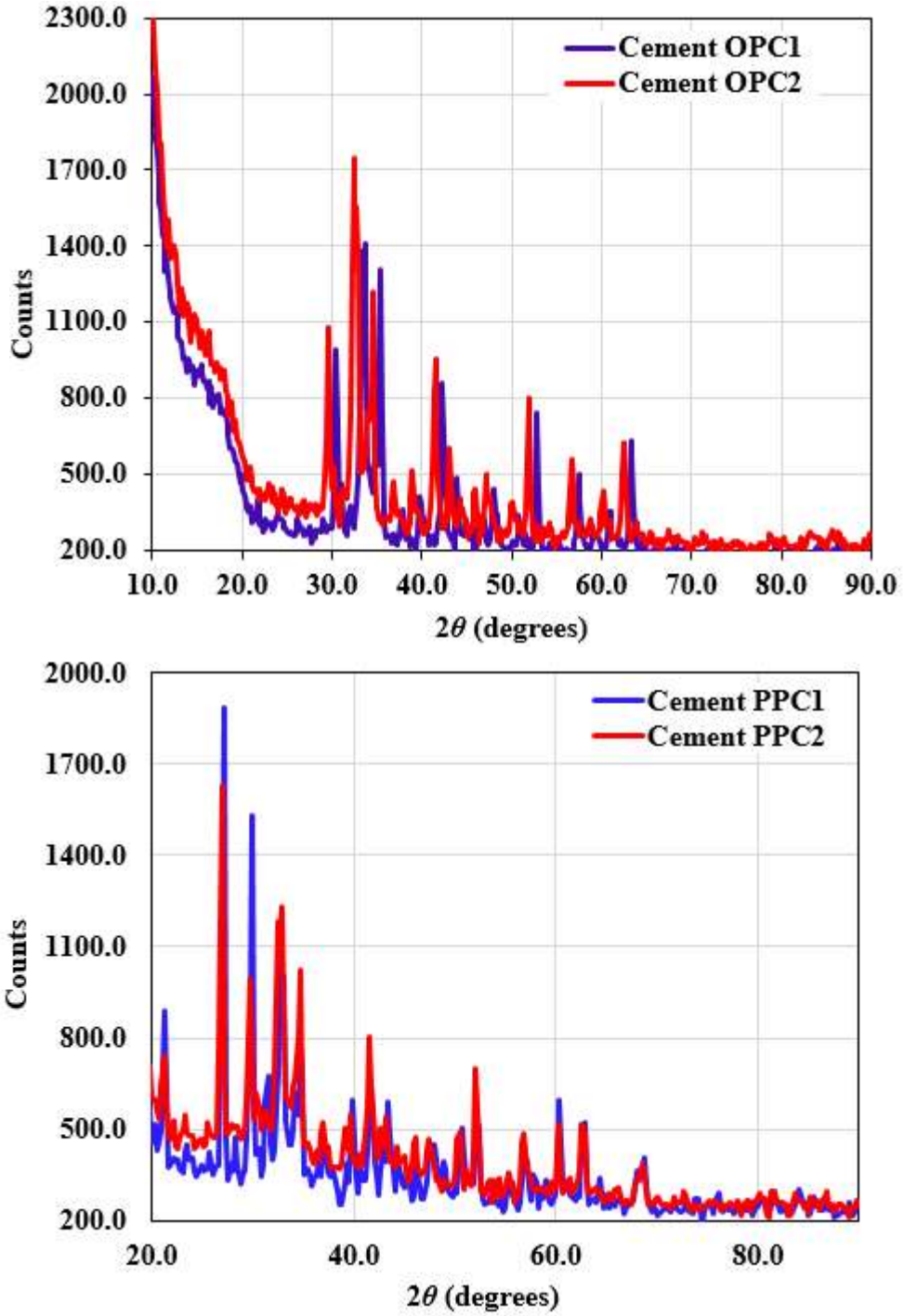

Figure 4. Comparisons of the XRD diffractograms between the OPC (OPC1 & OPC2), and PPC (PPC1 & PPC2) cements produced in Nepal.

therewith derived net integral area (A) values (mm^2) by incorporating the spectral intensity height (H) and FWHM (β) variables (Eq. 1) are mentioned in the insets of the corresponding figures separately. For easy analyses, they are tabulated in Table 1 as well wherein the predominant crystallite phases speculated from the particular value of the $2\theta_{max}{}^{0}$ are also mentioned sidewise. By explicit comparisons of the magnitudes of the A (mm^2) determined for the most predominant crystallite phases of the OPC and PPC cements, we confirm that PPC1 (A = 443 mm^2) contains almost 1.5 times more quantitative amounts of the portlandite, alite, aragonite, and vaterite type crystallite phases than in the PPC2 (A = 305.22 mm^2), and the OPC1 (A = 196 mm^2) contains a little bit more quantity of the calcite and other polymorphic phases than in the OPC2 (A = 187 mm^2). Among the OPC and PPC cement themselves, the latter one has an exceedingly higher percentage yet contrasting predominant crystallite phases owing to have the relatively more intense (H) and/or wider FWHM (β) spectral band than in the former as compared in Figure 3.

In general, the high intensity XRD peaks means more superposition of the constructive and destructive interferences caused basically by the variable atomic positions, and the atomic layouts guided peak intensities always showcase the existence of the dissimilar crystal lattice in the particular crystallite phases [32] as observed in the PPC and OPC. More than this, the broader XRD peaks with the higher β exemplify that there is a presence of the more non-uniform compressive and tensile strains plus higher disorder in the crystal lattice of the predominant crystallite phases as noted in the present PPC (PPC1: β = 0.2661º, PPC2: β = 0.2355º) samples relative to the OPC (OPC1: β = 0.2237º, OPC2: β = 0.2119º). The next supportive evidence for this greater degrees bulk and lattice defects exist in the PPC crystallites is the appearance of the more non-uniform shapes, higher degree asymmetricity, and *Gaussian* unlike distributions in its prominent XRD band as observed in Figure 5. Therein, however, the relatively more uniform, narrower, and extra-symmetrical shaped peaks are seen for the OPC cement samples if the corresponding extrapolated regions are incorporated precisely. These interpretations are well agreeable as the alite (belite) phases of the cements are recognizably known with their highly (relatively less) defective crystallites and imperfect microstructures, and the percentage compositions of them are more predominant in the PPC cement brands [33]. In fact, such type disparate crystallite phases with high degree distortions and irregularities in the crystal lattices make the PPC cements exhibiting unequal hydration affinities, dissolution rates, nucleation reactions, and setting propensities to that of the OPC. Additionally, if the FWHM (β) and H variables that lead the net integral area A of the remaining subsidiary spectral bands of the PPC and OPC (Figure 3) arising alongside of their prominent bands are compared tentatively, the basic structural units, functional domains, and the specific crystallite phases typical to their extravagant cementitious features are again marked distinctly. These rigorous judgements verify that some of the functions of the PPC are superior than the OPC and vice versa, and so are to be employed them under the specified engineering tasks and the associated domains. The genuine comparisons between their temporally hydrated mortar pastes employed for the diverse engineering attributes would be more wise for rating their exclusive performances, however, the natures of the generic crystallite phases and their quantitative amounts based interpretations made here are quite acceptable for claiming their unequal functions and hydration propensities. The subsection 3.1.1.4 and 3.1.1.5 deduce more crucial roles of the FWHM (β) for granting the crystallite

International Journal of Progressive Sciences and Technologies (IJPSAT)
ISSN: 2509-0119.

https://ijpsat.org/
Vol. 50 No. 1 April 2025, pp. 01-26

& grain sizes, and their growth propensities by means of which the water permeability and wettability plus the overwhelming hydration affinity aspects of the OPC and PPC cement grains can be rated more practically.

3.1.1.4 Crystallite Size (L_c) and Growths

The Scherrer's formula (Eq. 3) is a straightforward mathematical subordinate that can incorporate the β (rad) value of the particular spectral band arousing at the specific X-ray diffraction angle (θ^0) directly, and enables us to estimate the minimum crystallite size (L_c) appropriately. As per its formulation, the L_c value of the particular crystallite phase (microstructural domain) is inversely proportional to the magnitudes of the corresponding XRD spectral profile descriptors β and θ. Since determining the β values explicitly for every individual diffraction bands protruding at the particular $2\theta^0$ angle are tedious yet impractical, the most prominent

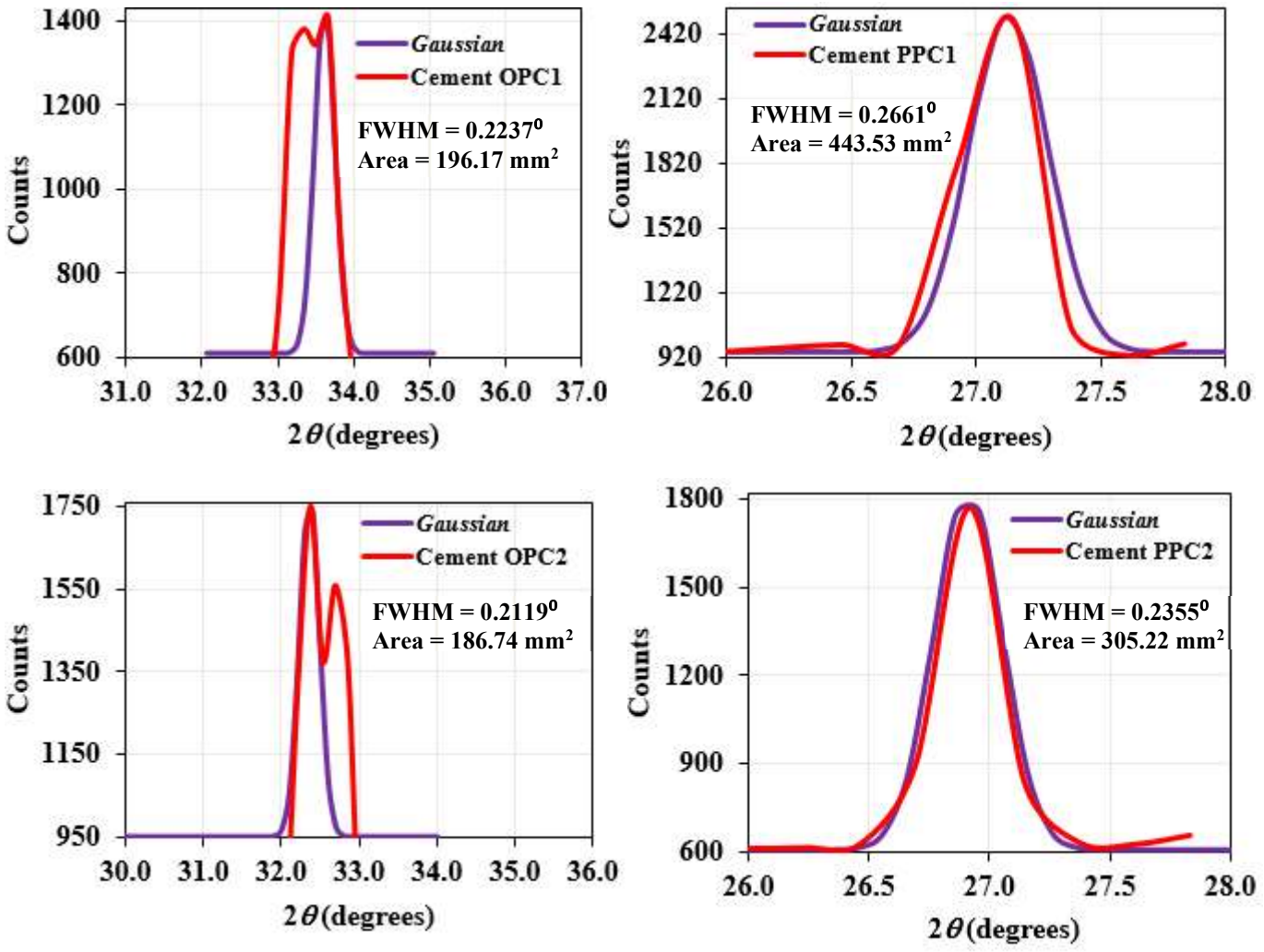

Figure 5. The *Gaussian* convolution fitting of the most intense XRD peaks (marked in **Figure 2** and **Figure 3**) of the cement samples: (a) OPC1 with $2\theta = 33.66°$, (b) PPC1 with $2\theta = 27.15°$, (c) OPC2 with $2\theta = 32.38°$, and (d) PPC2 with $2\theta = 36.92°$. Therewith determined FWHM (β) and area (A) under the peaks are mentioned in the respective insets.

spectral bands indicative to the predominant crystallite phases of the OPC and PPC cements arousing at the specific $2\theta_{max}$ diffraction angles are undertaken herewith just to assess their full widths at half maxima. The required $\theta = 2\theta_{max}/2$ and the *GAUSS* function peak-fitting (Figure 5) derived β values are summarized in Table 1 wherein the calculated values of the L_c are listed out sidewise. In the XRD investigations of the cement like materials and concrete mixtures, such a directly measurable quantity L_c serves as a standalone descriptor not only for theorizing the agglomerations tendencies of their particulate crystallites and basic structural units but also for approximating their grain cum particle sizes. These materials properties in fact determine the real-world physical observables of the cements such as particulates packing ratios & void volume, weight & density, water permeation & hydration/rehydration reaction trends, water-cement intermixing affinities, homogeneities in the binder paste matrices, scratch resilient nanogel embedded surface endurances, and the overall plasticity & hardening aptitudes of the mortar pastes [4]. Additionally, the frequency of the pre- and post- curing and the periodical treatments/caring of the mortar pastes with water (at least for 28 days), their water retaining and subsequent rehydration abilities, and thereafter acquiring exceptional hardening strengths, and concreting features are also directly dependent on the crystallite cum grain sizes and growths [5]. In the periphery of these ideologies, if the minimum L_c values calculated for the most predominant crystallite phases of the OPC (OPC1: L_c = 39 nm; OPC2: L_c = 41 nm) and PPC (PPC1: L_c = 32 nm; PPC2: L_c= 36 nm) cements are analyzed coherently, the relatively better crystallites sizes and growths are observed in the former type cements; granting that the PPC contains more extra fine crystallite phases with better material diffusivity propensities and longer hydration reaction rates. The greater L_c values of the OPC indirectly showcase us that the concerned crystallite phases possess relatively more weakly cross-linked interatomic layers (i.e. more departed layers with larger *d*-space as discussed in subsection 3.1.1.2) than in the PPC. This is because the larger *d*-space crystallite phases holding relatively less tightly packed and loosely bound interatomic layers with better parallel layouts (more perfectness, and less disorderliness) always lead to the facile breakages of their interlocking binding forces and hence, more rigorous restructurings of the greatly departed atomic layers do occur internally. The same microstructural phenomena are the eventual causes for explaining the variable growth kinetics and agglomerations rates: the PPC crystallites are less defect free with more disordered atomic layers than the OPC causing the former to undergo less facile internal restructurings and rearrangements than the latter (subsection 3.1.1.3). Saying this, the L_c values estimated here simply represent the minimum crystallite sizes of the OPC and PPC cements as the corresponding XRD bands undertaken herewith are only the most intense which are not necessarily to have a wider β and a larger diffraction angle (θ) than those assigned to other subsidiary bands. But, they are still lying in the acceptable range if the concerned literature datasets are referred: the calcite based cements have $L_c \approx$ 20–60 nm [34], boehmite alumina high percentage cements have $L_c \approx$ 3nm–60 nm [35]. Nevertheless, if the agglomerated grain sizes approximated from the same minimum L_c values are interpreted, the PPC in general has a feebly comparable or lower dimensional basal plane grains cum particles to that of the OPC. It is because the smaller L_c always agglomerates into the smaller grain cum particle sizes: the grains are the collection of the crystallites of identical orientations or are simply the assembly of such a single-domain structural unit. This observation is in accordance with the fineness of the pozzolanic ingredients and the natures of the clinkers chemical phases employed in the PPC production industrially. The same extreme grains sizes and ultrafine crystallite particulates utmost make the PPC cement powder matrices to (a) own recognizably lower permeability & accessibility, and hence offer higher durability & enduring strengths, (b) undergo slow hydration processes with less heat of hydration, and hence more suitable for mass castings & concreting of the engineering structures, (c) offer denser and compact concrete structures, and hence better shrinkage controls, (d) acquire slower setting times (initial: 30 min (OPC and PPC), and final: 600 min (OPC:280 min) [36]), and hence administer better mortar pastes spreading, surface finishing & homogeneity, weather resiliencies, and chemical (alkalis, sulfates, chlorides, acid rain etc.) attack preventions along with the successive hardening of the structures as a function of setting time.

3.1.1.5 Number of Parallel Interatomic Layers (*m*)

The next indicator that can verify the existences of the crystallite phases predominantly in the both OPC and PPC cements is an *m*; a numeral value that quantifies the minimum number of the weakly crosslinked parallel interatomic layers (from the (002) reflection) held into the particular crystallite phases. It has a direct relation with the L_c and an inverse relation with the *d*-space as shown in

Eq. 5; means it physically measures the minimum thickness of the particular crystallite phase comprising with the definite number density of the parallel atomic layers. The calculated values of it for each individual OPC1, PPC1, OPC2, and PPC2 cement samples are tabulated in Table 1; OPC1: m = 174, PPC1: m = 177, OPC2: m = 190, and PPC2: m = 202; reconfirming that the cement samples having the bigger crystallite sizes L_c and/or smaller d-space do possess higher number density of the parallel atomic layers. These are the good evidences to reclaim that plentiful number densities of the atomic layers do exist in the particular predominant crystallite phases of the both type cements which in fact are the basic structural units taking part in the internal rearrangements and restructurings in the course of evolving into the bigger crystallites. Actually, in the immediate hydration reactions of the cement grains with the proper quantity of water (w/c is usually 0.3–0.5), the newly derived non-uniform sized C–S–H nanogel glues (needle shaped, 1D nanomaterial) get adsorbed at first superficially on the grains cum particles, and progressively acquires bigger & bigger sizes (rod-shaped, 1D), denser matrices plus finer diffusivities without sudden change in the morphological textures [37], the thickness of the crystallites cum grains of the cements matters a lot towards exhibiting this unique characteristic features. The finer mass depositions and spreading plus the better growth orientations of the C–S–H (I) and C–S–H (II) gel nanoparticles do take place whenever the dimensions of the cement grains cum particles are bigger, and therefore the gluing abilities & plasticity properties of the cement and/or mortar pastes are directly enhanced even in the early hydrations periods. S. Meng *et al.* observed that the 5μm dimension cement particles adsorb the substantial number density C–S–H nanoparticles than that of the 500 nm diameter particle at 15 min. hydration periods, and the same trends continue even the hydration time prolongs to 4 hr. [37]. In this context, the presently determined minimal thicknesses of the particular crystallite phases are obviously admissible (m = 90–270 (calcite based cement) [34]; m = 3–100 (boehmite alumina cement) [35]; $m \geq 100$ (alite based cements [38])) owing to render enough exposures and effective adsorbing surface areas more especially to the poor crystallinity and short-range characters holding immature stage C–S–H nanoparticles because of which all the aftermath setting chemistries of the cement particles route to the facile proceedings. More particularly, the presently estimated slightly larger edge plane thickness (m) of the PPC crystallites cum grains/particles relative to the OPC allows us to speculate that its secondary hydration reaction leading to the C–S –H (II) nanogel formation is quite feasible and generous as they can finely adsorb the C–S–H (I) gel produced earlier in the primary hydration steps, and drive rest of the processes efficiently. The same is the reason the smaller d-spaced, larger edge plane thickness (m) yet finer particulates, and more defective & imperfective crystallite phases alike to that present in the alite, belite, and portlandite in descending order are highly preferred in cement productions industry as we discussed earlier: the premiere crystallite particulates of the PPC cements showing high degree imperfectness always enhance the heterogeneous nucleation processes, dissolution & hydration mechanisms, and aggregation properties of the C–S–H nanoparticles more pronouncedly that the OPC (the effects of the turbostratic order of the crystallites and the nanoconfinement of the C–S–H nanoparticles are not undertaken here seriously) [39, 40]. Though the Scherrer analyses always assume the spherical crystallite shapes, and the in-depth chemical interactions between the adsorbing chemical species on the hydrating cement particles are not known yet fully, the currently depicted interdependencies between the grains thicknesses and the adsorbing tendencies of the fresh C–S–H nanogels on their effective surface area, and thereafter evolving cementitious features would be the great deal of evidences in understanding dissimilar workability of the OPC and PPC cements.

3.1.2 Chemical Moieties and Effectiveness of the FTIR Method

All the X-ray diffraction spectroscopy profile assessments identified disparate crystallite phases present in the OPC and PPC cement grains are furthermore confirmed herewith by FTIR spectroscopy technique. Unlike in the XRD, the FTIR spectral characterizations always trace out the specific IR spectral bands arise from the infrared active vibration modes of the heteroatomic chemical bonds exist in any types of the heteroatomic functional moieties and bonding fragments of the particular chemical phases. As per its selection rule, the IR active chemical bonds are designated to those that undergo change in dipole moments upon the absorption of the specific wavelength IR radiations, and the polar covalent bonds between the heteroatoms always fulfill this criteria by exhibiting genuine vibrational transitions within the framework of typical IR frequency regions (400 cm^{-1}–4000 cm^{-1}). More than this, the covalent bonds with the higher (lower) percentage polarity character always vow to produce the intense and strong (medium and weak) vibration bands, and the combination bands are often observed when more than one polar bond vibration transitions of the similar or dissimilar chemical moieties occur at the identical IR frequency regions [20, 21]. Since the OPC and PPC cement materials are comprising with the dissimilar regime basic structural units and functional chemical phases holding identical and/or nonidentical

International Journal of Progressive Sciences and Technologies (IJPSAT)
ISSN: 2509-0119.

https://ijpsat.org/
Vol. 50 No. 1 April 2025, pp. 01-26

heteroatomic chemical moieties disproportionally, the exact applications of the FTIR spectral measurement techniques to trace out them explicitly and the precise examinations of their IR active vibration bands always lead to the absolute presumptions of their generic functioning aptitudes and functionalizing qualifications in a semiquantitative scale. The same spectral characterizations and the associated interpretations would be the most indispensable microstructural assets in proclaiming their contrasting functionalizing practices and serviceability in different architectural designs and engineering constructions. Additionally, the exclusive markings of the chemical fragments and functional groups held into the founding crystallite phases of the grainy powder cement matrices through the successive usage of the IR spectroscopy technique forecast the most probable chemical compounds and product derivatives to be released upon their proceedings of the hydration and rehydration reactions progressively. Therefore, the FTIR

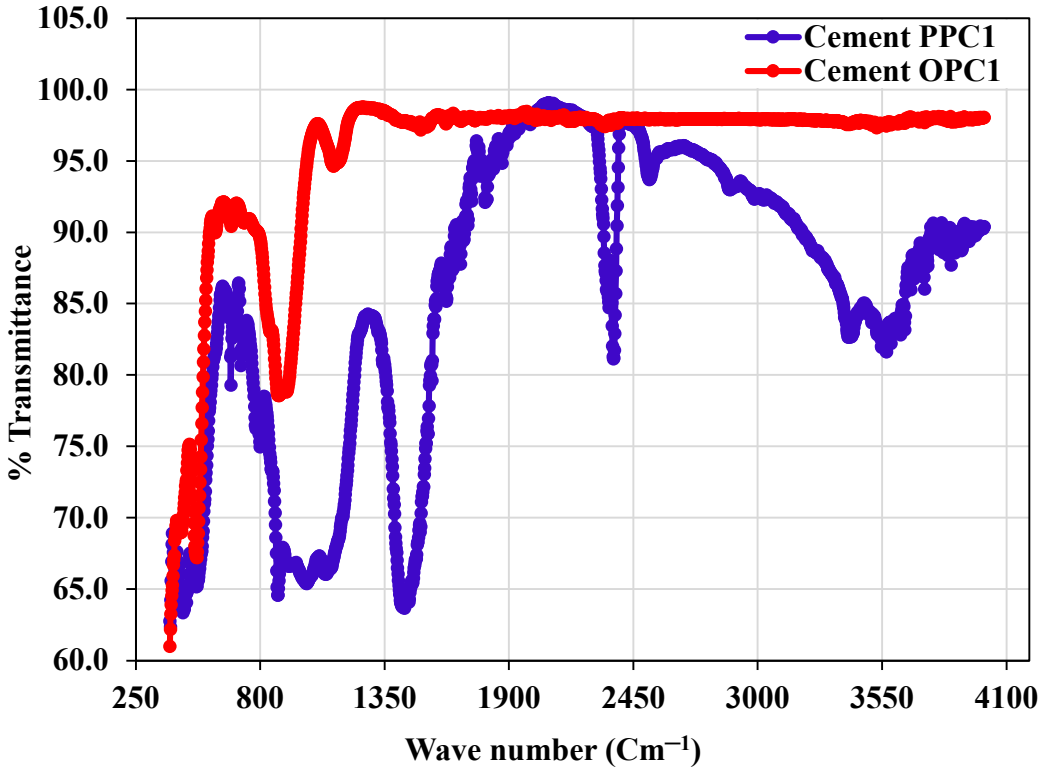

Figure 6. Comparisons of the FTIR spectrograms between the cement samples OPC1 and PPC1 produced by the same manufacturer. The most intense IR bands are appeared at (a) OPC1: ~500 cm^{-1}, ~520 cm^{-1}, 870 cm^{-1}—920 cm^{-1}, 1140 cm^{-1}, and (b) PPC1: 400 cm^{-1}, ~520 cm^{-1}, ~800 –1100 cm^{-1}, ~1440 cm^{-1}, ~1800 cm^{-1}, ~2360 cm^{-1}, ~2530 cm^{-1}, ~3420 cm^{-1}, ~3560 cm^{-1}, ~3850 cm^{-1}.

spectroscopy deserves good recognitions in cement and concrete research if it is employed along with the additional spectroscopic tools for getting the complete characterizations of the specific cement materials.

3.1.2.1 Identifications of the IR Active Vibration Bands

The FTIR spectra measured for the presently selected Nepal-made cement samples OPC1 & PPC1, and OPC2 & PPC2 are plotted comparatively in Figure 6 and Figure 7 respectively wherein all the predominant IR active vibration bands are clearly visible at contrasting absorption frequency regions. The easily identifiable IR absorption frequency (wavenumber, cm^{-1}) regions for the each

International Journal of Progressive Sciences and Technologies (IJPSAT)
ISSN: 2509-0119.

https://ijpsat.org/
Vol. 50 No. 1 April 2025, pp. 01-26

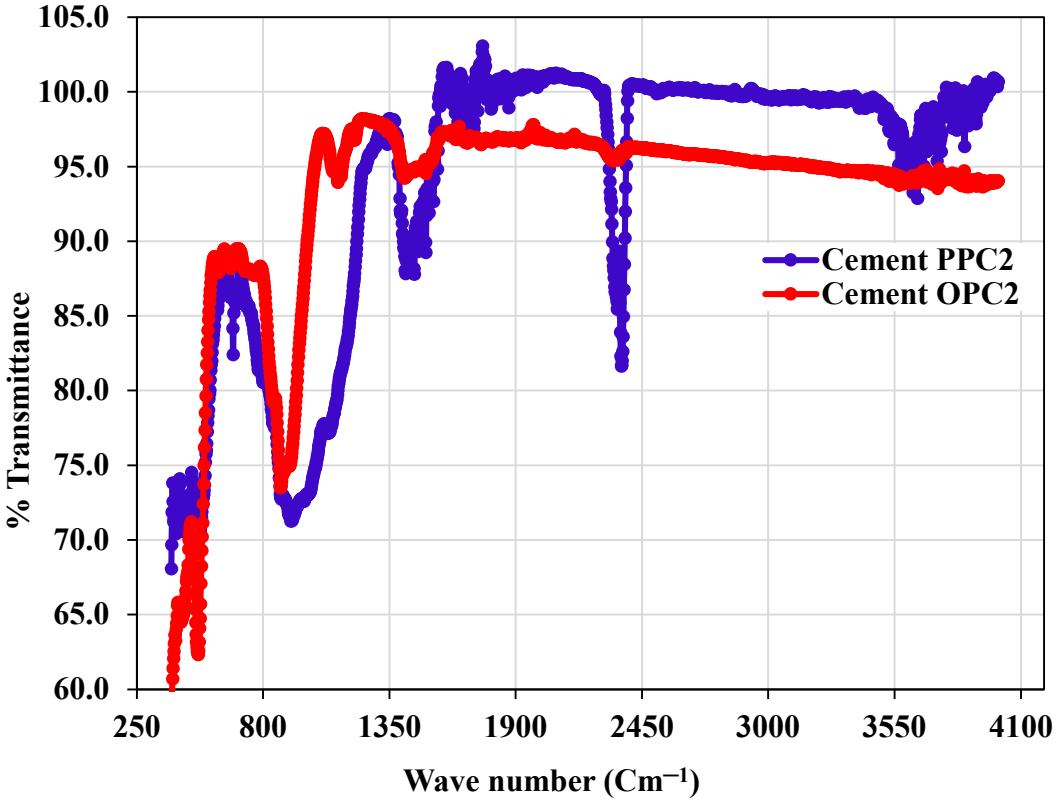

Figure 7. Comparisons of the FTIR spectrograms between the cement samples OPC2 and PPC2 produced by the same manufacturers. The most intense IR bands are appeared at (a) OPC2: ~500 cm^{-1}, ~520 cm^{-1}, ~870 cm^{-1}—920 cm^{-1}, ~1400 cm^{-1}, ~1510 cm^{-1}, ~2350 cm^{-1}, ~3740 cm^{-1}, and (b) PPC2: ~450—520 cm^{-1}, ~670 cm^{-1}, ~920 cm^{-1}, ~1100 cm^{-1}, ~1460 —1870 cm^{-1}, ~2360 cm^{-1}, ~3650 cm^{-1}.

and every discernible spectral bands are; (a) OPC1: ~500 cm^{-1}, ~520 cm^{-1}, ~870 cm^{-1}—~920 cm^{-1}, ~1140 cm^{-1}; (b) PPC1: ~400 cm^{-1},~520 cm^{-1}, ~800 cm^{-1} –~1100 cm^{-1}, ~1440 cm^{-1}, ~1800 cm^{-1}, ~2360 cm^{-1}, ~2530 cm^{-1}, ~3420 cm^{-1}, ~3560 cm^{-1}, ~3850 cm^{-1}; (c) OPC2: ~500 cm^{-1}, ~520 cm^{-1}, ~870 cm^{-1} — ~920 cm^{-1}, ~1400 cm^{-1}, ~1510 cm^{-1}, ~2350 cm^{-1}, ~3740 cm^{-1}; and (d) PPC2: ~450 cm^{-1} — ~520 cm^{-1}, ~670 cm^{-1}, ~920 cm^{-1}, ~1100 cm^{-1}, ~1460 cm^{-1} — ~1870 cm^{-1}, ~2360 cm^{-1}, ~3650 cm^{-1}. Based on these spectral positions of the concerned IR bands, and their spectral depth intensity (percentage transmittance) & rigorous fingerprint patterns, we presume that the PPC cements contain relatively more wide-range heteroatomic bonding groups with higher percentage bond-polarity (more electronegative atoms) and microstructural functional domains than in the OPC. It further speculates that some of the predominant chemical phases owned by the former brands are of clearly distinguishable types to those of the latter as their dissimilar range fingerprint regions always reveal the uniqueness in bonding patterns between the heteroatoms with quirky layouts and structural arrangements. However, the principal spectral fingerprint regions and the absorption frequency regimes observed in the OPC only (OPC1 & OPC2), and PPC only (PPC1 & PPC2) IR spectra are quite similar as plotted together in Figure 8: the more diligent probing and spectral interpretations, rigorous specifications of the functional domains, and the exact quality accreditations amongst the variable brands Nepal made OPC and PPC cements are reported herewith [23, 29, 30] by the same authors. Therein, both of these cement brands are assessed thoroughly based on the Nepal standard (NS) codes, globally adopted industrial formulations, and the Bogue compositions for optimizing the cement qualities. Therefore, the hereafter discussions are fully

concentrated into the comparative crystallite phases and their heteroatomic bonding moieties in OPC and PPC that actually lead these cements to dispense variable engineering functions, cementitious features, and conscientious roles.

3.1.2.2 Comparisons of the Chemical Moieties and Bonding Fragments

Within the frameworks of the IR spectra, spectral bands, and therewith correlated fingerprint regions assigned to the specific bonding fragments of the particular crystallite phases, the generic chemical compositional variations existing in the OPC and PPC cement grains are compared as follows. For the OPC cements, the IR active regions at (a) ~500 cm^{-1} – ~520 cm^{-1} (strong and sharp bands), ~600 cm^{-1}, ~670 cm^{-1} (weak and diffuse bands); the positions designated to the out-of-plane Si−O bending in silicate (SiO_4^{2-}) and its polymorphs, (b) ~615 cm^{-1} (weak and diffuse); indicative to the traces of Al–O and Al−OH vibrations in alumina and aluminate compounds (tricalcium aluminate, calcium dialuminate), (c) ~870 cm^{-1} – ~876 cm^{-1} (strong and sharp); the typical positions to the out of plane bending vibration modes of the CO_3^{2-} functional groups in amorphous calcite ($CaCO_3$) and vaterite phases, and As–O active vibration modes in arsenate compounds (Pharmacolite, $CaHAsO_4 \cdot 2(H_2O)$) [41, 42], (d) ~920 cm^{-1} (weak and diffuse); the specific positions for the asymmetric Si−O stretching vibrations in the silicate compounds, (e) ~ 600 cm^{-1} – ~680 cm^{-1} (weak and diffuse), and ~1120cm^{-1} – ~1140 cm^{-1} (strong, sharp but lower depth); the characteristic positions to the O−S−O

International Journal of Progressive Sciences and Technologies (IJPSAT)
ISSN: 2509-0119.

https://ijpsat.org/
Vol. 50 No. 1 April 2025, pp. 01-26

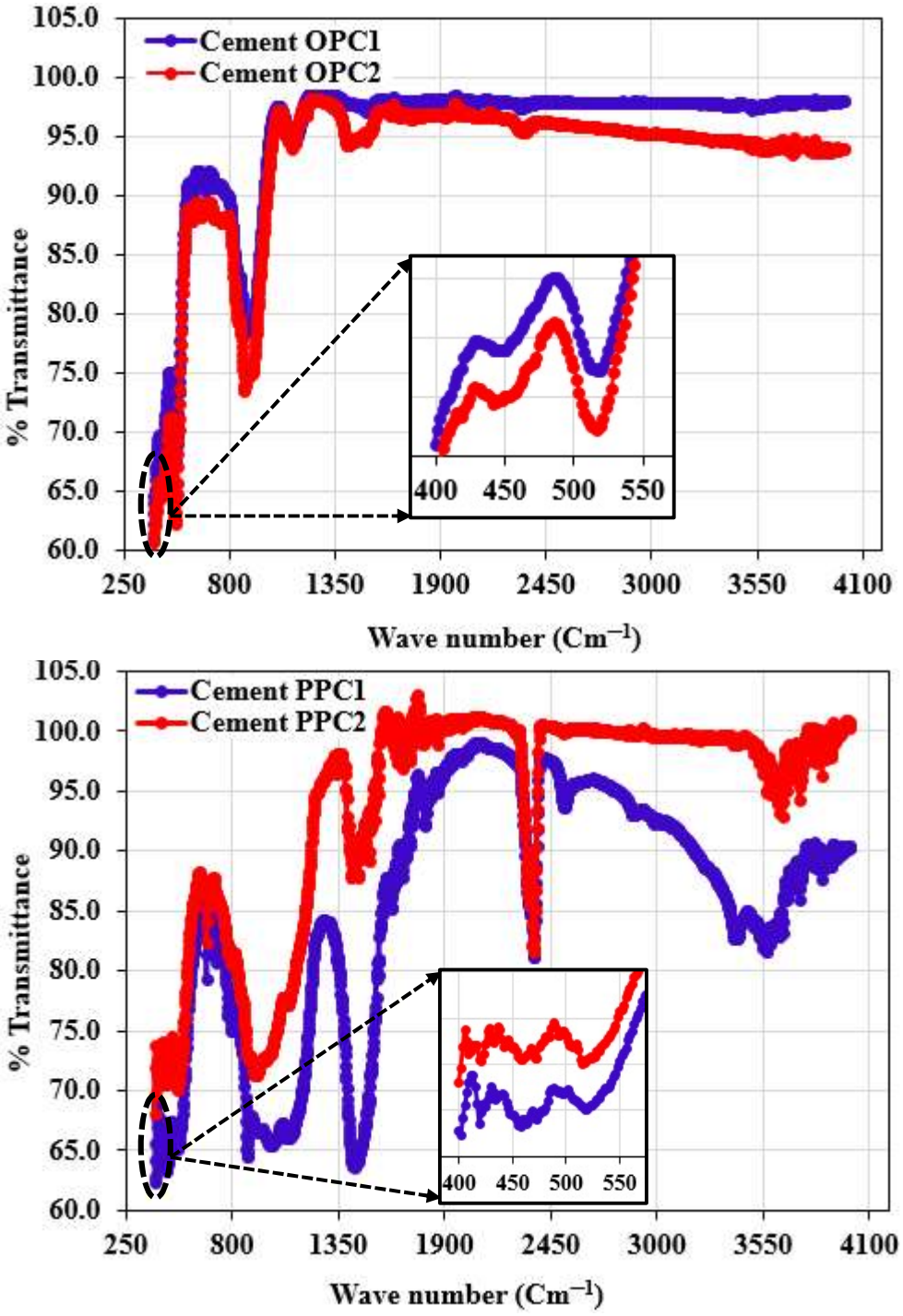

Figure 8. Comparisons of the FTIR spectrograms between the OPC (OPC1 & OPC2), and PPC (PPC1 & PPC2) cements produced in Nepal.

bending modes in gypsum ($CaSO_4 \cdot 2H_2O$), Mg–O stretchin g modes in magnesium oxide (MgO), active vibration modes of AlO_4–tetrahedral and AlO_6–octahedral in aluminoferrite phases [43], and O–S stretching modes of the SO_4^{2-} in sulphate

International Journal of Progressive Sciences and Technologies (IJPSAT)
ISSN: 2509-0119.

https://ijpsat.org/
Vol. 50 No. 1 April 2025, pp. 01-26

compounds (Bassanite, $2CaSO_4 \cdot H_2O$; Aphthitalite, $K_3Na(SO_4)_2$) respectively, (f) ~445 cm^{-1} (weak and diffuse); H−O−H vibration modes in gypsum liberated water traces plus Mg−O (MgO) and Si–O–Si (SiO_2) symmetric bending vibrations [20, 21, 27]. But, for the PPC cements, the IR active regions are at (a) ~ 400 cm^{-1} – ~ 420 cm^{-1} (weak and diffuse); the Ca–O stretching vibration modes in fly ash (CaO) phases, (b) ~ 470 cm^{-1} (weak and diffuse) and ~1100 cm^{-1} (strong and sharp); the Si–O–Si bending vibration modes in silica (SiO_2, α-quartz) phase and Si–O asymmetric stretching modes in silicate moieties (alite (Ca_3SiO_5), and belite (Ca_2SiO_3) phases) respectively, (c) ~520 cm^{-1} and ~ 670 cm^{-1} (weak and narrow); Si–O–Si symmetric bending vibration modes (shifted from ~ 450 cm^{-1} region due to being the gypsum as one of the ingredients), and S–O stretching vibrations of SO_4^{2-} unit in $MgSO_4$–fly ash/slag matrix & gypsum plus Mg−O stretching modes in magnesium oxide (MgO) respectively, (d) ~713 cm^{-1} (weak and diffuse); CO_3^{2-} deformation vibrations in aragonite, (e) ~880 cm^{-1} (sharp and narrow); the combination band for the As–O active vibration modes (ν_3 AsO_4^{3-}) in the As^{5+}–bearing calcium arsenate compounds: $CaH_4(AsO_4)_2$, $CaH(AsO_4)$, $Ca_3(AsO_4)_2$, & $Ca_5(AsO_4)_3OH$, and out-of-plane CO_3^{2-} bending vibrations (ν_2 CO_3^{2-}) in light calcite ($CaCO_3$) and its polymorphic forms, (f) ~920 cm^{-1}, and ~970 cm^{-1} (sharp and wide); the asymmetric Si–O stretching vibration modes of the primary silicate phases, and of calcium silicate hydrate Ca (Si–O–H) respectively; (g) ~1000 cm^{-1}, ~1100 cm^{-1}, and ~1120 cm^{-1} (acute and narrow); the ν_3 SiO_4^{4-} & ν_3 SiO_4^{2-} of the tetrahedral moieties in the silicates and their polymerized moieties (orthosilica $(Si_2O_7)^{6-}$), CO_3^{2-} stretching vibrations in aragonite, and SO_4^{2-} stretching vibrations in the sulphate compounds (gypsum, Bassanite) plus few active vibration modes in the aluminoferrite phases respectively; (h) ~1440 cm^{-1} (strong and narrow); the stretching C–O vibration modes (ν_2 CO_3^{2-}) of the CO_3^{2-} unit in calcite, aragonite, and vaterite, (i) ~1800 cm^{-1} (weak and diffuse) and ~2360 cm^{-1} (strong and sharp); the C=O vibration modes of the CO_3^{2-} segment in the calcite and O–C–O stretching modes of the CO_2 (CO_2 infused from the atmosphere adds $CaCO_3$ traces due to its chemical reaction with the portlandite phase; $Ca(OH)_2 + CO_2 \rightarrow CaCO_3 + H_2O$) respectively, (j) ~2530 cm^{-1} (medium and low depth), and ~2880 cm^{-1} (weak and diffuse); combination (ν_3+ν_4) and $2\nu_3$ vibration modes of the CO_3^{2-} part in $CaCO_3$ polymorphs, (k) ~3420 cm^{-1} (medium and low depth); asymmetric O–H (portlandite $Ca(OH)_2$ phases), H–O–H (crystal waters of the hydrated calcites ($CaCO_3.nH_2O$) and gypsums ($CaSO_4.2H_2O$)), and/or hydrogen bond inbound O–H segments stretching, (l) ~3600 cm^{-1} – ~ 3645 cm^{-1} (weak and diffuse); typical to the low degree carbonated cement but enriched with the portlandite phases, and (m) ~3850 cm^{-1} (weak and diffuse); C–H vibration modes of the pozzolanic organic traces (PPC utilizes impure natural and non-natural pozzolana as its precursor raw materials).

As a whole, all these IR spectral comparisons not only overview the predominant as well as the subsidiary level crystallite phases present in the both OPC and PPC cement grains, quantify their generic heteroatomic chemical moieties consisting of the polar covalent bonds, and foresee the reasons behind their unequal working performances as deduced earlier through the XRD spectroscopy (subsection 3.1.1) but also illuminate their disparate cementitious features underlying into the plasticity properties of the mortar pastes, binding and gluing potentialities, hydration and rehydration reactions affinities, stabilizing and hardening abilities, concreting and enduring aptitudes, compressibility and hair-crack preventions, chemicals and weather attack resiliencies, etc. Beside this, these explicit yet comparative deductions of all the founding chemical constituents of the OPC and PPC cements may guide the industrial specialists to optimize the cementitious features in their commercial products along with successive suspecting of the most probable hardening chemical compounds to be released in due course of setting time progressively upon reacting with the evaporable water sieved into their mortar pastes. More than this, all the insightful spectral comparisons and the relevant discussions made through the IR spectroscopy are very much appropriate to specify the reasons of ongoing variable functionalizing inclines and applicability of the OPC and PPC cements in the general commercial markets and engineering constructions.

4. CONCLUSION

The direct applications of the instrumental techniques to characterize the dissimilar functioning cements comprising with the distinctive clinker phases, crystallites particulates, and chemical moieties are quite apparent in cement and concrete research. But, the exclusive investigations of the disparate functional qualifications, variable workability, and distinguishable cementitious features of ultra-dry ready-to-use grainy OPC and PPC cement powders simply by assessing their crystallites microstructures and the associated coherent domains through the multifaceted spectroscopic means are still greatly conceded. In this contribution, we carried out the XRD and FTIR spectroscopy profile assessments of the specifically selected Nepal made OPC and PPC cements

separately, and probed into their versatile microstructural domains and therewith dependent applicative qualifications & functionalizing aptitudes semiquantitatively. The descriptive spectroscopic parameters that were undertaken comprehensively in order to take into account of all these indispensable assets are XRD peak positions, *d*-space (basal spacing), shapes & intensity (H) of the selected diffraction bands, FWHMs (β) & net integral area (A) of the prominent peaks, size of the crystallites (L_c) & their growth propensities, number density of the interatomic layers & edge plane thicknesses of the predominant crystallite phases, and the FTIR spectral bands fingerprint to the definite functional groups & chemical moieties of the particular crystallites.

Based on the diffraction angles, diffracted peak positions, and therewith identified crystallite materials analyses of the OPC and PPC cements, we speculated their quite contrasting founding chemical compositions and clinker phases preliminarily. The explicit comparisons between each of their crystallite phases and functional chemical constituents implicated us to theorize that they do possess disproportional quantity basic structural units and functional domains, so they tend to offer dissimilar functionalizing qualifications and applicative aptitudes under distinctive engineering conditions. We confirmed each of these phases through their *d*-space values, and noticed that the relatively more (less) tightly packed crystallites present more predominantly in the OPC (PPC) granular cores would be their ultimate causes of exhibiting contrasting engineering functions and cementitious features. The similar type phase variations and disparities in them were also critically marked through their diffraction bands- shape and symmetry analyses: the PPC crystallites have the more non-uniform & wider-β band-shapes, taller intensity (H) & intensive interferences superposed diffraction bands, greater integral band-area (A), and higher degree asymmetry & *Gaussian* unlike distributions while the OPC crystallites have such bands exactly opposite to these spectral features; justified that the former cement contains highly defective crystallite phases with recognizable compressive and tensile strains in more quantity compared to the latter. These evidences supported us to proclaim that they do have unequal dissolution rates in water, hydration affinities, and hardening strengths in the due courses of setting time and progressive rehydration reactions. Additionally, the strengths of the crosslinking forces that bind the *d*-spaced interatomic layers into their particular crystallite phases were also presumed by estimating the L_c values and growth kinetics: the relatively larger (smaller) L_c values determined for the OPC (PPC) not only depicted their weakly (strongly) cross-linked interatomic layers and poorly (greatly) disordered crystallite phases but also deduced its better (poorer) agglomeration rates cum grain size evolutions trends. This observation ensured us that the OPC (PPC) cements own recognizably higher (lower) water permeability & accessibility with faster (slower) hydration and rehydration processes both in the early and late stages. More than this, the XRD derived edge plane thicknesses of their defective predominant crystallites allowed us to claim that the PPC (OPC) grains possess more (less) specific adsorbing sites and exposable surface areas onto which the finer (poorer) mass depositions & spreading plus better (worse) growth orientations of the C–S–H (I) & C–S–H (II) silicate hydrate nanogels and their aftermath hardening procedures do occur facilely. At last, the entire crystallite phases in them and their isolated chemical fragments were reaffirmed insightfully through the rigorous FTIR spectral judgements and fingerprint vibration bands assessments. We believed that therewith derived complimentary spectral information became the great deal of evidences not only to reconfirm their XRD speculations but also to illuminate their discrete cementitious functions and functionalizing inclines under diverse engineering perspectives and environmental scenarios.

DATA AVAILABILITY STATEMENT

The entire datasets used to verify the findings of this study are available from the corresponding author upon reasonable request.

ETHICS STATEMENT

This article does not contain any studies with human participants or animals. It has neither been published by any other journals nor currently under their consideration.

CONFLICTS OF INTEREST

The authors declare no conflicts of interests.

FUNDING

No financial support was received for this insightful analyses.

ACKNOWLEDGEMENT

The entire spectroscopic measurements were carried out in Nepal Academy of Science and Technology (NAST), Ministry of Education, Science and Technology, Kathmandu, Nepal.

DISCLAIMER (ARTIFICIAL INTELLIGENCE)

Author hereby declares that no generative AI technologies and text-to-image generators have been used during writing or editing of this manuscript.

REFERENCES

[1]. P. K. Mehta, P. J. Monteiro, Concrete: Microstructure, Properties, and Materials (McGraw-Hill Education; 2013).

[2]. S. H. Kosmatka, B. Kerkhoff, W. C. Panarese, Design and Control of Concrete Mixtures (5420 Old Orchard Road Skokie, Illinois; 2008).

[3]. A. M. Neville, Properties of Concrete (Pearson Education; 2011).

[4]. T. Staněk, P. Sulovský, M. Boháč, *Cem. Concr. Res.*, 92, 21(2017).

[5]. C. Mounira, *J. Cem. Based Compos.*, 1, 7(2021).

[6]. (a) K. Prasain, Nepal will require 26 million tonnes of cement annually by 2024-25, *The Kathmandu Post*, 2021. Available online: https://kathmandupost.com/money/ 2021/05/21/nepal-will-require-26-million-tonnes-of-cement-annually-by-2024-25-report-says#:~:text=Krishana%20Prasain&text=Nepal%20is%20estimated%20to%20require,Rastra%20Bank%20on%20Friday%20showed (accessed on 3/24/2025).

(b) Nepal become self-reliant in clinker, *Khabarhub*, 2019. Available: https://english. khabarhub.com/2019/09/53872/ (accessed on 3/24/2025).

[7]. Top 12 Nepali Cement Brands 2024, 2024. Available online: https://insightsnp.com/top-12-nepali-cement-brands-2023/ (accessed on 3/24/2025).

[8]. (a) Nepal cement worth 170 million exported, *Rastrita Samachar Samiti*, 2023. Available online:https://nepalnews.com/s/business/nepal-cement-worth-170-million-exported#:~:text=Two%20Nepali%20cement%20industries%20have,cement%20since%20October%2017%2C%202022 (accessed on 3/24/2025).

(b) D. Paudel, Increase in cement exports raises hope in Nepal's foreign trade, *Myrepublica Nagariknews*, 2024. Available: https://myrepublica.nagariknetwork.com/news/increase-in-cement-exports-raises-hope-in-nepal-s-foreign-trade/ (accessed on 3/24/2025).

(c) Nepal (Imports and Exports): Trade Economy. Available online: https://trendeconomy. com/data/h2/Nepal/6810) (accessed on 3/24/2025).

(d) Once a heavy cement importer, Nepal is now an emerging exporter. Available online: https://ansuinvest.com/research-opinion/view/nepal-once-a-heavy-cement-importer-is-now-an-emerging-cement-exporter115 (accessed on 3/24/2025).

[9]. P. R. Pandey, N. Banskota, *Bul. Dep. Geol. Trib. Univ.*, 11, 71(2000).

[10]. P. Banstola, K. K. Shrestha, I. Thapa, A. K. Mishra, *Int. J. App. Eng. and Management. Lett.* 5(2), 26(2021).

[11]. Department of Geology and Mines, Nepal. Feasibility of clays in Nepal for use in Limestone Calcined Clay Cement (LC). Available: *chrome-extension:// efaidnbmnnnibpcajpcglclefindmkaj/https://www.tara.in/assets/pdf/blue-white-modern-profesional-business-flyer.pdf* (accessed on 3/24/2025).

[12]. (a) R. Maskey, Energy Use in Nepalese Cement Industries: Case of Udayapur Cement Industries Limited, 2016. Available: https://www.academia.edu/68371430 (accessed on 3/24/2025)

(b) Ordinary Portland cement market size & share analysis - growth trends & forecasts up to 2030. Available: https://www.mordorintelligence.com/industry-reports/global-ord inary-portland-cement-market (accessed on 3/24/2025)

[13]. (a) Ordinary Portland cement (OPC) Market Size and Forecast. Available: https://www.verifiedmarketresearch.com/product/ordinary-portland-cement-opc-market/ (accessed on 3/24/2025)

(b) Blended Cement Market to Reach $462.1 Billion, Globally, by 2031 at 4.2% CAGR: Allied Market Research. Available: https://www.prnewswire.com/news-releases/blended-cement-market-to-reach-462-1-billion-globally-by-2031-at-4-2-cagr-allied-market-research-301767856.html (accessed on 3/24/2025)

[14]. A. Jayaswal, *Int. Res. J. Mod. Eng. Tech. Sci.*, 3(3), 871(2021).

[15]. R. L. Amhudo, T. T. Raka, I. G. Putu, *Civil Eng. Journal*, 4(8), 1760(2018).

[16]. J. H. Bhatt, P. D. Prajapati, Khalak A. Abarar, P. J. Mehul, *Intl. J. Res. Pub. Rev.* 4(12), 1105(2023).

[17]. M. Berra, T. Mangialardi, A. E. Paolini, *Adv. Mat. Sci. Eng.* 4853141, 1(2018).

[18]. A. Singh, S. Gupta, J. Singh, N.P Singh, *Int. J. Res. Eng. Tech.*, 4(5), 60(2015).

[19]. R. Vedalakshmia, A. Sundara Rajb, S. Srinivasana, K. G. Babu, *Thermochimica Acta* 407, 49(2003).

[20]. M. Y. A. Mollah, M. Kesmez, D. L. Cocke, *Sci. Total Environ.*, 262, 25(2004).

[21]. M. Y. A. Mollah, F. Lu, D. L. Cocke, *Sci. Total Environ.*, 224, 57(1998).

[22]. L. A. Silva, B. O. Nahime, E. C. Lima, J. L. Akasaki, I. C. Reis, *Cerâmica,* 66(380) 373(2020).

[23]. A. B. Marahatta, G. Baral, K. Dhital, *International Journal of Progressive Sciences and Technologies*, 45(2), 01(2024).

[24]. N. N. Kencanawati, S. Rawiana, N. P. R. Darmayanti, *Aceh Int. J. Sci. Tech.*, 9(1), 40(2020).

[25]. J. I. Langford, J. C. Wilson, *J. App. Cryst.*, 11, 102(1978).

[26]. D. M. Smilgies, *J. App. Cryst.*, 42, 1030(2009).

[27]. National Research Council, National Academy of Sciences, National Academy of Engineering. Guide to compounds of interest in cement and concrete research, 1972 (pp. 1-63). Available online: https://onlinepubs.trb.org/Onlinepubs/sr/sr127.pdf (accessed on 3/24/2025).

[28]. E. T. Carlson, Some Properties of the Calcium Aluminoferrite Hydrates, Building Research Division, Institute of Applied Technology, U. S. Department of Commerce, National Bureau of Standards, Washington, D.C. Available online: chrome-extension://efaidnbmnnnibpcajpcglclefindmkaj/https://nvlpubs.nist.gov/nistpubs/Legacy/BSS/nbsbuildingscience6.pdf (accessed on 3/24/2025).

[29]. G. Baral, A. B. Marahatta, *Asian J. Appl. Chem. Res.*, 14(4), 34(2023).

[30]. A. B. Marahatta, P. K. Dahal, *International Journal of Progressive Sciences and Technologies*, 46(2), 83(2024).

[31]. S. Condurache-Bota, C. Gheorghies, A. P. Rambu, A. M. Cantaragiu, *Annals of the "Dunărea de Jos" University of Galaţi – Fascicle ii*, 142(2009).

[32]. F. Girgsdies, Peak Profile Analysis in X-ray Powder Diffraction. Available: chrome-extension://efaidnbmnnnibpcajpcglclefindmkaj/https://www.fhi.mpg.de/1075438/frank_girgsdies__peak_profile_fitting_in_xrd__151106.pdf (accessed online: 3/24/2025).

[33]. R. K. Mishra, R. J. Flatt, H. Heinz. *Phys. Chem. C*, 117(20), 10417(2013).

[34]. V. Lilkov, O. Petrov, D. Kovacheva, I. Rostovsky, Y. Tzvetanova, V. Petkova, N. Petrova, *Constr. Build. Mater.*, 124, 838(2016).

[35]. Baxter S, United States Patent Application US 2014/0224156A1; 2014. Available online: https://patentimages.storage.googleapis.com/96/5a/fb/da13658a1555e3/US9056791.pdf (accessed on 3/24/2025).

[36]. J. D. Waghmare, S. S. Pati, S. M. Patil, M. M. Maske, *ASEAN J. Sci. Engg.*, 1(1), 13(2021).

[37]. S. Meng, X. Ouyang, J. Fu, Y. Niu, Y. Ma, *Nanotechnol. Rev.*, 10, 768(2021).

[38]. P. E. Stutzman, P. Feng, J. W. Bullard, *J. Res. Nat. Inst. Stand. Tech.*, 121, 47(2016).

[39]. G. Artioli, J. W. Bullard, *Cryst. Res. Technol.* 48(10), 903(2013).

[40]. R. Pellenq, N. Lequeux, H. V. Damme, *Cem. Concr.Res.*,38(2),159(2008).

[41]. L. Badurina, B. Segvic, O. Mandic, G. Zanoni, *Minerals*, 10(10), 899(2020).

[42]. P. Głuchowski, R. Tomala, D. Kujawa, V. Boiko, T. Murauskas, P. Solarz, *J. Phys. Chem. C*, 126(16), 7127(2022).

[43]. L. F. Carrasco, D. T. Martín, L.M. Morales, S. M. Ramírez, Infrared Spectroscopy-Analysis of Building and Construction Materials, 370-381(Intechopen, Rijeka; 2012).